

Magnetic Excitations in Bilayer High-Temperature Superconductors with Stripe Correlations

G.S. UHRIG^{1*}, K.P. SCHMIDT¹ and M. GRÜNINGER²

¹*Institut für Theoretische Physik, Zülpicher Straße 77, Universität zu Köln, 50937 Köln, Germany*

²*Physikalisches Institut, RWTH Aachen, 52056 Aachen, Germany*

The universal behaviour of the magnetic excitations in high-temperature superconductors is described in a model with static stripes retaining only the localized spin degrees of freedom. The stripes are represented by a model of coupled two-leg spin ladders. We start from the results obtained previously by continuous unitary transformations for an isolated spin ladder. A quantitative description of neutron scattering data is reached, using a model for a single cuprate layer with well established values of the exchange coupling constants. The neutron resonance peak is explained in terms of a saddle point in the dispersion of the magnetic excitations. Here we make predictions for bilayer systems with in-phase or out-of-phase stripe correlations. The results may serve as a guide for future experimental analyses.

KEYWORDS: magnetic excitations, spectral densities, stripe phase, inelastic neutron scattering, high-temperature superconductors

1. Introduction

The rôle of the magnetic excitations in the mechanism of high-temperature superconductivity is still heavily debated. A prerequisite for a successful understanding of this rôle is a quantitative description of the magnetic excitations themselves. For many years, however, it seemed that different families of compounds display rather different behaviour of their magnetic excitations.^{1–3} Recent experimental evidence for a universal behaviour of the magnetic excitations^{4–6} clearly indicates the relevance of these features and calls for detailed theoretical investigations.

Phenomena In the single-layer compound $\text{La}_{2-x}\text{Sr}_x\text{CuO}_4$ (LSCO), four incommensurate satellites are observed in elastic neutron scattering experiments at low temperatures. These satellites are shifted away from the antiferromagnetic wave vector $\mathbf{Q}_{\text{AF}} = (1/2, 1/2)$ in reciprocal lattice units (rlu). In the insulating phase at low doping ($p \lesssim 6\%$), the shift occurs along the diagonal while it occurs parallel to the tetragonal reciprocal axes in the superconducting phase ($p \gtrsim 6\%$).^{7,8} The size of the shift is roughly linear in the doping p for small values of p . It saturates at about $1/8$ of the Brillouin zone for sizeable doping levels ($p \gtrsim 10\%$),^{8,9} see also Fig. 1.4 in Ref.¹⁰ These incommensurate features may be explained in terms of the superstructure satellites of a stripe phase (see below), which is supported by the observation of the corresponding charge-order satellites around the Bragg peaks in Nd-doped LSCO.^{11,12} Incommensurate magnetic excitations were observed in LSCO also in *inelastic* neutron scattering (INS) experiments.^{6,13–18}

In the bilayer compound $\text{YBa}_2\text{Cu}_3\text{O}_x$ (YBCO_x), the magnetic response at optimum doping is dominated below T_c by the resonance peak at \mathbf{Q}_{AF} with an energy of $\omega_{\text{res}} \approx 41$ meV.^{1,3,19} The observation of a resonance peak at \mathbf{Q}_{AF} below T_c with $\omega_{\text{res}} \approx 47$ meV in single layer $\text{Ti}_2\text{Ba}_2\text{CuO}_y$ ²⁰ shows that the bilayer structure is not a

prerequisite for the occurrence of the resonance peak. Incommensurate branches have been observed at low energies in the underdoped regime and more recently also at about optimal doping.^{21–25} Elastic superstructure satellites indicating charge order were also reported in underdoped YBCO,²⁶ suggesting that also this system may display an instability towards stripe formation. A third feature is the appearance of incommensurate branches *above* the resonance energy.^{21,23–26}

Universality The data for YBCO provide evidence that the resonance peak and the incommensurate excitations are not separate features but form part of the common dispersive magnetic excitations of the cuprate high-temperature superconductors. Very recently, this point of view has been substantiated by reports on very similar INS data obtained on $\text{YBCO}_{6.6}$ ⁴ and $\text{La}_{15/8}\text{Ba}_{1/8}\text{CuO}_4$ (LBCO),⁵ both at low and at high energies in a large part of the Brillouin zone. On the one hand, the experiment of Tranquada and co-workers on LBCO⁵ provides data for a *charge-ordered* phase which suppresses the superconducting phase.^{27,28} The data show the incommensurate excitations which are familiar in the La family. Additionally, a dominant feature is observed at \mathbf{Q}_{AF} , which is the first report of such a resonance in this family. In contrast to YBCO, the resonance in LBCO is observed in the normal (charge-ordered) state. On the other hand, the experiment by Hayden and co-workers for $\text{YBCO}_{6.6}$ displays very similar features.⁴ Yet the system is in the *superconducting* state. Recently, Christensen *et al.* pointed out the similarity of the dispersion in the superconducting phases of optimally doped LSCO and YBCO.⁶

These findings suggest that the magnetic excitations in the high- T_c cuprate superconductors are of universal character. Differences may stem from the differences in the state of the charges. The absence of a resonance peak in LSCO may be explained by the position of the resonance mode with respect to the particle-hole continuum. If the decay into particle-hole pairs is fast the magnetic

*E-mail address: gu@thp.uni-koeln.de

modes may be overdamped so that they are not seen in experiment as prominent peaks.^{29,30} In fact, the incommensurate magnetic excitations in LSCO become much sharper upon cooling.^{14,15}

Modulated Phases An appealing route to account for the important features of the magnetic excitations sketched above is to assume a certain long-range charge modulation. This implies a corresponding superstructure in the spin sector which in turn leads to periodicities different from those of the underlying lattice. The most prominent modulation considered is the formation of stripes. It was proposed theoretically in the late eighties^{31,32} on the basis of the energy gain due to binding of charges to domain walls. Later such modulations were observed experimentally in, e.g., nickelates,^{33,34} and cuprates.¹¹

While there are certain cuprate systems for which the existence of static stripes is well established, e.g., rare-earth-doped LSCO,^{11,12,35} there are others which do not appear to display static long-range stripes, for instance optimally doped YBCO. We like to emphasize, however, that there are theoretical predictions based on phenomenological dimer models which show that even very small charge modulations can have a sizeable effect on the spin sector, e.g., inducing a significant modulation of dimer correlations.³⁶ So it is not excluded that certain charge orderings eluded so far experimental observation because of their smallness.

Recent experiments on an *untwinned* sample of slightly underdoped YBCO_{6.85}³⁷ have not found a significant anisotropy in the weights of the incommensurate peaks. The data display a certain anisotropy regarding the peak width. Assuming that a given orthorhombic domain determines the orientation of a possible stripe order these findings do not support the existence of a static one-dimensional stripe pattern, but they may be consistent with fluctuating stripes. For a further discussion of the physics of static or dynamic stripes we refer to Refs.^{1,10,38,39}

Stripe Pattern The stripe phase corresponds to a segregation into hole-rich and hole-poor ribbons. Experimentally, a doping dependence of the periodicity has been reported in elastic neutron scattering experiments on underdoped LSCO.^{8,9} The shift of the magnetic satellites away from \mathbf{Q}_{AF} saturates at about $1/8$ for larger doping levels ($p \approx 0.1$), see e.g. Fig. 1.4 in Ref.,¹⁰ corresponding to a spin superstructure periodicity of $8a$ where a is the in-plane lattice constant. The concomitant charge superstructure periodicity of static stripes is found to be $4a$.^{11,12} This is the periodicity we choose in our model. The spin superstructure of $8a$ can be explained by, e.g., assuming that the hole-rich ribbons form anti-phase domain walls for the spins, corresponding to an effective *ferromagnetic* coupling between the spins across a hole-rich stripe (see below).

In the literature, two patterns of stripe modulation are studied. One is the site-centered pattern where the hole-rich stripe is a chain, i.e. the width of this stripe is only one site. Neighbouring hole-rich stripes are separated by three hole-poor sites with localized spins, which can be viewed as a three-leg spin ladder. This pattern

is the one that was considered mostly.¹ But an attractive alternative is the bond-centered pattern where the hole-rich stripe has a width of two sites. These stripes are separated by two hole-poor spin sites, corresponding to a two-leg spin ladder (see Fig. 1). There is evidence from band structure calculations that the bond-centered modulation is favourable.⁴⁰ Moreover, the magnetic state is more stable in the bond-centered pattern than in the site-centered one because spin ladders with an even number of legs are gapped^{41,42} and thus stable against small perturbations. Spin ladders with odd number of legs are critical^{41,42} and thus highly unstable against any perturbation or spontaneous symmetry breaking. A quantum Monte-Carlo study illustrates that in the bond-centered pattern much of the fluctuations originate directly in the spin sector while in the site-centered pattern the interplay between spin and charge sector is essential.⁴³

Another interesting piece of evidence in favour of the bond-centered scenario can be derived from the Fourier analysis of the modulations observed by scanning tunneling microscopy (STM)⁴⁴ on underdoped $\text{Ca}_{2-x}\text{Na}_x\text{CuO}_2\text{Cl}_2$. We interpret the data here as resulting from the spatial average of vertical and horizontal stripes. A discussion of a possible truly two-dimensional 4×4 tiling modulation is left to future research. The STM data show features at $\pm 1/4$ rlu, but not at $1/2$ rlu. The bond-centered modulation with period $4a$ is indeed generated by a single cosine term with wave vector $2\pi/4a$; no higher harmonics appear. In contrast, the general site-centered modulation with period $4a$ is characterized by the fundamental and the first harmonic. Hence, the generic site-centered modulation should display a feature also at $1/2$ rlu. Thus the STM data rather support the bond-centered scenario.

Theoretical Approaches There are many theoretical approaches to the magnetic excitations in the cuprate superconductors.² They can be split into two classes:

(i) Starting from an underlying *fermionic* model, mostly extended Hubbard models, one has to deal with strong interactions. The magnetic collective modes appear in the particle-hole or particle-particle channel. In essence, they are bound states or resonances of two fermions.² Widely used techniques in this field are approaches based on random phase approximations (see e.g. Ref.⁴⁵ and references therein), and renormalization schemes (see e.g. Refs.⁴⁶⁻⁴⁸). The regime of strong interactions with coupling constants larger than the band width is difficult to describe reliably.

(ii) Alternatively, one may start from a bosonic model which contains the collective modes already from the very beginning. Then the interplay with the charge degrees of freedom is added by some coupling. The approaches based on spin-fermion models^{29,49} or many treatments of t - J models^{50,51} are of this type. In the very limit, the fermionic excitations are neglected, focusing on the collective modes alone (see e.g. Refs.^{52,53}).

In the present work we use an approach of the second type. We discuss a spin-only Heisenberg model of coupled spin ladders with effective coupling parameters, assuming that the charge degrees of freedom are integrated out. Roughly speaking, the excitation energies of

the charge degrees of freedom are of the order of t while the magnetic energies are of the order of $J \approx t/3$. So it makes sense to consider an effective magnetic model at low energies with the faster charge degrees of freedom being eliminated. One has to keep in mind that the decay of the magnetic collective modes into particle-hole pairs is neglected which will certainly play a rôle at higher energies. Neglecting this decay is well justified in the superconducting state where the charge excitations are mostly gapped.

While we start from a spin-only model with long-range stripe order our predictions are equally relevant for systems with fluctuating stripe order for not too low energies. The time scale of these fluctuations should be above the time scale set by the inverse energy of the features under study.

Vojta and Ulbricht⁵⁴ investigated the same spin-only model without the cyclic spin exchange (see below) by a mean-field approach starting from dimers on the rungs of the ladders. The description of isolated ladders is improved by a local energy correction which accounts for a part of the effect of the hard-core constraint of the excitations on each dimer. The constant-energy scans in this approach agree qualitatively with the results we obtained for a single-layer model.^{55,56}

In a phenomenological approach Vojta and Sachdev considered also a plaquette modulation.⁵⁷ From their results they concluded that the magnetic excitations of a plaquette modulation do not agree with the inelastic neutron data.^{4,5}

Seibold and Lorenzana performed a large-scale time-dependent Gutzwiller calculation for a Hubbard model to determine the magnetic excitations of a stripe phase with charge and spin order.⁵⁸ Using parameters adapted to describe the magnetic dispersion of the undoped system and the doping dependence of the incommensurability they find good agreement with the inelastic neutron data for LBCO. The similarity between their constant-energy scans and those from spin-only approaches suggests that the damping due to the charge degrees of freedom does not play an essential rôle in the presence of charge and spin order. We presume that this is due to a partial freezing out of the charge degrees of freedom.

Aim of this Study and Set Up It is the aim of the present study to extend our previous investigations based on long-range stripe modulations in a single layer^{55,56} to bilayer cuprates such as YBCO. In addition, further results for single layers will be presented. All these results provide valuable guiding predictions for present and future inelastic neutron scattering experiments.

The article is set up as follows. In the next section, Sect. 2, the model will be introduced and its theoretical treatment will be explained. In Sect. 3 results for single layers will be presented. In the subsequent Sect. 4, results for two different modulation patterns in bilayers will be shown and compared. In Sect. 5 various scans at constant energy will be given. Finally, the conclusions will be drawn in Sect. 6.

2. Model and Calculation

Model In the Introduction we have motivated to consider the single-layer model sketched in Fig. 1. The Hamiltonian H is conveniently split into an intra-ladder part H_{ladder} and an inter-ladder part H_{inter}

$$\begin{aligned} H_{\text{ladder}} = & \sum_{i \in \Gamma} J_{\perp} \mathbf{S}_i^L \cdot \mathbf{S}_i^R + J_{\parallel} (\mathbf{S}_i^L \cdot \mathbf{S}_{i+\delta_y}^L + \mathbf{S}_i^R \cdot \mathbf{S}_{i+\delta_y}^R) \\ & + J_{\text{cyc}} \sum_{i \in \Gamma} [(\mathbf{S}_i^L \cdot \mathbf{S}_i^R)(\mathbf{S}_{i+\delta_y}^L \cdot \mathbf{S}_{i+\delta_y}^R) \\ & + (\mathbf{S}_i^L \cdot \mathbf{S}_{i+\delta_y}^L)(\mathbf{S}_i^R \cdot \mathbf{S}_{i+\delta_y}^R) - (\mathbf{S}_i^L \cdot \mathbf{S}_{i+\delta_y}^R)(\mathbf{S}_{i+\delta_y}^L \cdot \mathbf{S}_i^R)] \end{aligned} \quad (1)$$

where the superscripts L and R stand for the left and the right spin on a rung, respectively. The subscript $i = (i_x, i_y)$ denotes the rung by pointing to its center, i.e. the mid-point between the left (L) and the right (R) spin. The possible values are $\Gamma = a(4\mathbb{Z}, \mathbb{Z})$. The shift δ_y is given by $(0, a)$. The coupling between the spin ladders reads

$$H_{\text{inter}} = J' \sum_{i \in \Gamma} \mathbf{S}_i^R \cdot \mathbf{S}_{i+4\delta_x}^L, \quad (2)$$

where $\delta_x = (a, 0)$. As in the previous work we consider the isotropic spin ladder with $J := J_{\perp} = J_{\parallel}$ because the system is derived from a square lattice. The cyclic exchange (J_{cyc}) is known to be the dominant correction to the nearest-neighbour Heisenberg spin exchange.^{59–61} In the square lattice, its importance has been proposed⁶² and confirmed.^{63,64} Similarly, it has been proposed for two-leg spin ladders⁶⁵ and could be confirmed by the analysis of two-triplet bound states.^{66,67} We will use the thus established value $J_{\text{cyc}} = 0.2J_{\perp}$. Taking J_{cyc} into account is crucial if one aims at a quantitative agreement with experimental data.^{55,56} The effective exchange constant J' across the hole-rich stripes depends on the state of the eliminated charge degrees of freedom. The presence of holes substantially reduces J' relative to J .⁵⁵

In practice, we will fit J' to the experimental data; it takes a small ferromagnetic value ($J' < 0$) of a few percent of J .^{55,56}

Next we extend the above model from a single layer to a bilayer. We consider the two possibilities depicted in Fig. 2. There are, of course, still other patterns which can be considered. We focus on those in Fig. 2 due to their high symmetry.

Denoting the spins in the second layer by the superscripts R' and L' the coupling between the two layers reads

$$H_{\text{in-phase}} = J_s^{\text{ip}} \sum_{i \in \Gamma} (\mathbf{S}_i^L \cdot \mathbf{S}_i^{L'} + \mathbf{S}_i^R \cdot \mathbf{S}_i^{R'}) \quad (3)$$

$$H_{\text{out-of-phase}} = J_s^{\text{oop}} \sum_{i \in \Gamma} (\mathbf{S}_i^L \cdot \mathbf{S}_{i-2\delta_x}^{R'} + \mathbf{S}_i^R \cdot \mathbf{S}_{i+2\delta_x}^{L'}) \quad (4)$$

The exchange coupling J_s^{ip} takes small antiferromagnetic values ($J_s^{\text{ip}} > 0$). It corresponds to the interlayer exchange J_s determined for the undoped parent compound YBCO₆^{68,69} so that it should have about the same value. In case of YBCO₆, a value of $J_s \approx 0.08J$ has been deduced from the observation of optical magnons at around 70 meV^{68,69} and from a comparison of the two-magnon spectra in Raman scattering and in the optical conduc-

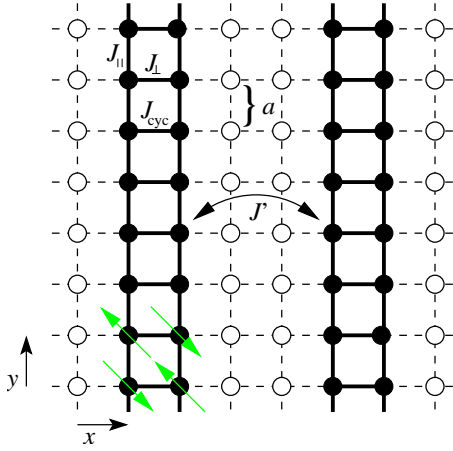


Fig. 1. Sketch of the model in a single cuprate plane. Each circle stands for a copper ion, i.e. the site of a spin 1/2 or a hole. The filled circles stand for the hole-poor regions where localized spins are assumed. The empty circles stand for the hole-rich stripes where itinerant behaviour is assumed. The spin-only model comprises only the localized spins which form a lattice of coupled two-leg ladders. The intraladder couplings are J_{\parallel} , J_{\perp} and J_{cyc} ; the interladder coupling J' is an effective coupling across the charged hole-rich stripes.

tivity.⁷⁰

In the coupling J_s^{oop} we do not denote the small superexchange processes to next-nearest neighbours. The coupling J_s^{oop} is an effective coupling which takes processes into account via the eliminated site (open circles in Fig. 2b). If there is a spin on the eliminated site there will be a ferromagnetic contribution to J_s^{oop} because both adjacent spins prefer to be antiparallel to it, hence parallel to each other. If the eliminated site is empty there will be an antiferromagnetic contribution to J_s^{oop} because the adjacent spins can undergo exchange processes. In total, the ferromagnetic and the antiferromagnetic contributions will partially cancel so that a small $|J_s^{\text{oop}}| < J_s^{\text{ip}}$ remains. Its sign is plausibly ferromagnetic since the eliminated site is occupied to 75% at doping 1/8. Note that the effective coupling J' between adjacent ladders was motivated in the same way.⁵⁵

Calculation: Single Layer The calculation runs in analogy to the one that we performed previously for the single layer.⁵⁵ A perturbative continuous unitary transformation (CUT) is performed for each ladder sep-

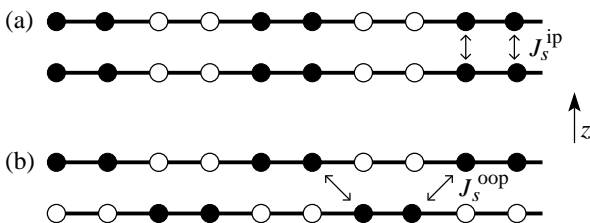


Fig. 2. Sideview of the two stripe-order patterns that we consider in bilayer systems (view along the y direction; open and full circles as in Fig. 1). The pattern in (a) assumes that the modulation is stacked; we will call this order in-phase. The pattern in (b) assumes that the modulation is alternating (out-of-phase).

arately.^{71, 72} Thereby, we obtain an effective model in terms of the elementary triplet excitations, triplons,⁷³ of the spin ladder. This effective model includes the one-triplon part $\sum_{k,\alpha} \omega_k^0 t_k^{\alpha,\dagger} t_k^\alpha$ where k is the wave vector along the ladder and $\alpha \in \{x, y, z\}$ is the flavour index for the three states of a triplon. The operator t_k^α stands for the annihilation of a triplon of flavour α with momentum k and $t_k^{\alpha,\dagger}$ stands for its creation. The dispersion ω_k^0 has been computed in many ways, see e.g. Refs.^{67, 71, 74–76} or Fig. 2a in Ref.⁵⁵

Besides the one-triplon part the effective model for the isolated ladder includes contributions involving two and more triplons. We neglect them since the one-triplon contribution dominates for the physically relevant parameters where 63% of the total spectral weight is in the one-triplon channel.⁵⁵

The coupling *between* the ladders can be written without a new comprehensive calculation. We apply the above unitary transformation U to each spin component at each site of a ladder yielding an effective observable

$$S_{i,\text{eff}}^{\alpha,\text{R}} := U^\dagger S_i^{\alpha,\text{R}} U = \sum_{m \in \mathbb{Z}} a_m (t_{i+m\delta_y}^{\alpha,\dagger} + t_{i+m\delta_y}^\alpha) + \dots \quad (5)$$

$$S_{i,\text{eff}}^{\alpha,\text{L}} = - \sum_{m \in \mathbb{Z}} a_m (t_{i+m\delta_y}^{\alpha,\dagger} + t_{i+m\delta_y}^\alpha) + \dots \quad (6)$$

Here t_i^α stands for the annihilation of a triplon of flavour α on the dimer i and $t_i^{\alpha,\dagger}$ stands for its creation. Consistent with the above approximation, the higher contributions involving two and more triplons are neglected.

First, we will use the identities (5) and (6) to find the transformed Hamiltonian for the interladder coupling. This can be done replacing the product of spin components $S_i^\alpha S_{i+4\delta_x}^\alpha$ by the right hand sides of Eqs. (5) and (6) taking into account that triplon operators on different ladders are involved. They are distinguished in real space by the x -component of i , i.e. i_x . In reciprocal space we use h for the momentum perpendicular to the ladders (k is the momentum along the ladders). This yields

$$H_{\text{inter}} = -J' \sum_{h,k;\alpha} d_{h,k} (t_{h,k}^{\alpha,\dagger} + t_{-h,-k}^\alpha) (t_{h,k}^\alpha + t_{-h,-k}^{\alpha,\dagger}) \quad (7)$$

where the minus sign results from the coupling of a right spin (on rung i) to a left spin (on $i+4\delta_x$). The momentum dependence is given by

$$d_{h,k} := \cos(8\pi h) a^2(k) \quad (8)$$

where h is measured in rlu; the cosine term captures the shift $4a$ from one ladder to the next one. The factor $a(k)$ is the Fourier transform of the coefficients a_m

$$a(k) = \sum_m \exp(i2\pi km) a_m. \quad (9)$$

The shape of the weight $a^2(k)$ has been illustrated in Fig. 2b in Ref.⁵⁵

The total Hamiltonian after the CUT and after the neglect of the multi-triplon parts is

$$H_{\text{ladder}} + H_{\text{inter}} = \quad (10)$$

$$\sum_{h,k;\alpha} \omega_k^0 t_k^{\alpha,\dagger} t_k^\alpha - J' d_{h,k} (t_{h,k}^{\alpha,\dagger} + t_{-h,-k}^\alpha) (t_{h,k}^\alpha + t_{-h,-k}^{\alpha,\dagger}).$$

It is bilinear in the triplon creation and annihilation operators so that it looks like a trivial one-particle problem. Unfortunately, this is not the case because the triplons are hard-core bosons. At maximum one of the three kinds may be present on a given rung. To make analytical progress, we exploit the fact that J' is small compared to the global energy scale J . Hence the off-diagonal terms such as $t_{-h,-k}^\alpha t_{h,k}^{\alpha,\dagger}$ and its hermitean conjugate are small and so will be the errors that are introduced by neglecting the hard-core constraint. If the hard-core constraint is neglected, that means the triplons are treated as ordinary bosons, the Hamiltonian (10) can be diagonalized by a standard Bogoliubov transformation. The resulting dispersion reads

$$\omega_{h,k} = \sqrt{(\omega_k^0)^2 - 4J'd_{h,k}\omega_k^0}. \quad (11)$$

Note that the omission of the hard-core constraint implies that there is only one mode per each momentum. The decay into two or more modes has been neglected. Thus we are dealing with a single-mode approximation.

At zero temperature, the dynamic structure factor $S_{h,k}(\omega)$ measures at which rate the system can be excited at a given momentum h, k and frequency ω . The excitation operator is the Fourier transform of the local spin components

$$S_{h,k}^\alpha = \frac{1}{\sqrt{N}} \sum_i e^{i2\pi(ki_x + hi_y)} \left(S_i^{\alpha,R} e^{i\pi h} + S_i^{\alpha,L} e^{-i\pi h} \right) \quad (12)$$

where we assume that the position of a rung is given by its center. Inserting Eqs. (5) and (6) leads to

$$S_{h,k}^\alpha = i \sin(\pi h) a(k) (t_{h,k}^{\alpha,\dagger} + t_{-h,-k}^\alpha). \quad (13)$$

The dynamic structure factor is the sum over all absolute excitation amplitudes squared, that means the square of the absolute values of the prefactors of the creation operators *after* the Bogoliubov diagonalization. The evaluation brings us to

$$S_{h,k}(\omega) = \sin^2(\pi h) a^2(k) \frac{\omega_k^0}{\omega_{h,k}} \delta(\omega - \omega_{h,k}). \quad (14)$$

If we add the contributions at negative frequencies proportional to $-\delta(\omega + \omega_{h,k})$ we may rewrite the expression as the imaginary part of a retarded response function

$$S_{h,k}(\omega) = -\frac{2}{\pi} \text{Im} \frac{\sin^2(\pi h) a^2(k) \omega_k^0}{(\omega + i0_+)^2 - \omega_{h,k}^2}. \quad (15)$$

The above formulae describe the single layer case.

Calculation: Bilayer Let us consider the in-phase pattern first. There is an obvious reflection symmetry between the two layers, cf. Fig. 2a. Hence the additional degree of freedom is accounted for most easily by distinguishing even ($\sigma = 1$) and odd triplons ($\sigma = -1$) with respect to the reflection. We will call this property the parity of the mode. The additional part of the Hamiltonian reads

$$H_{\text{in-phase}} = \quad (16)$$

$$J_s^{\text{ip}} \sum_{h,k,\sigma;\alpha} \sigma a^2(k) (t_{h,k,\sigma}^{\alpha,\dagger} + t_{-h,-k,\sigma}^\alpha) (t_{h,k,\sigma}^\alpha + t_{-h,-k,\sigma}^{\alpha,\dagger}).$$

We do not write down the remaining part of the Hamiltonian $H_{\text{ladder}} + H_{\text{inter}}$ because it is diagonal in σ ; it is given by Eq. 10 for each value of σ separately. The resulting dispersion depends on the parity σ ,

$$\omega_{h,k,\sigma}^{\text{ip}} = \sqrt{(\omega_k^0)^2 + 4a^2(k)\omega_k^0 (\sigma J_s^{\text{ip}} - J' \cos(8\pi h))}. \quad (17)$$

The corresponding dynamic structure factor depends on the parity σ only via the dispersion. So Eq. (15) is still applicable once $\omega_{h,k}$ is replaced by $\omega_{h,k,\sigma}^{\text{ip}}$.

Now we consider the out-of-phase pattern. There is no obvious reflection symmetry but a combination of reflection and translation symmetry. Let us assume that all the spin ladders lie in the same plane. Then the difference to the single layer calculation is the presence of the additional ladders located between those of a single layer. The exchange J' couples ladders at distance $4\delta_x$; the exchange J_s^{oop} couples spin ladders at distance $2\delta_x$. Then the whole problem has become a problem in a single plane. We can stick to the wave vector h which now is defined in a larger interval ($h \in [-1/4, 1/4]$ instead of $h \in [-1/8, 1/8]$) because also rungs with position i in $a(2\mathbb{Z}, \mathbb{Z})$ carry spins, not only those at $a(4\mathbb{Z}, \mathbb{Z})$. The additional contribution in the Hamiltonian is denoted

$$H_{\text{out-of-phase}} = -J_s^{\text{oop}} \sum_{h,k;\alpha} \cos(4\pi h) a^2(k) \cdot (t_{h,k}^{\alpha,\dagger} + t_{-h,-k}^\alpha) (t_{h,k}^\alpha + t_{-h,-k}^{\alpha,\dagger}). \quad (18)$$

where the cosine factor has half the argument of the cosine factor in Eq. (8) because the distance bridged is only half the one bridged by J' . The Bogoliubov diagonalization leads to the dispersion

$$\omega_{h,k} = \sqrt{(\omega_k^0)^2 - 4a^2(k)\omega_k^0 (J_s^{\text{oop}} \cos(4\pi h) + J' \cos(8\pi h))}. \quad (19)$$

Equations (18) and (19) start from the doubled Brillouin-zone interval for the transverse momentum h . In order to compare the in-phase and the out-of-phase patterns as closely as possible we prefer to stay with the Brillouin-zone interval of the in-phase pattern. The part of the branch of the out-of-phase pattern which is located at $|h| \in [1/8, 1/4]$ is folded back by the shift $h = h' \pm 1/4$. The backfolded branch can be identified with the *odd* one because the phase factor from a ladder in the lower layer to a ladder in the upper layer is $\exp(4\pi i h) = -\exp(4\pi i h')$, that means there is an extra factor -1 as it is characteristic for the odd mode. In the dispersion, we distinguish the two branches by $\sigma = \pm 1$

$$\omega_{h,k,\sigma}^{\text{oop}} = \sqrt{(\omega_k^0)^2 - 4a^2(k)\omega_k^0 (\sigma J_s^{\text{oop}} \cos(4\pi h) + J' \cos(8\pi h))}. \quad (20)$$

Note that we simplified the notation by passing from h' back to h . The corresponding dynamic structure factor is again the same as in the single layer calculation (15) except that $\omega_{h,k}$ is replaced by $\omega_{h,k,\sigma}^{\text{oop}}$. Note that the substitution $h \rightarrow h \pm 1/4$ does not apply to the sine-factor

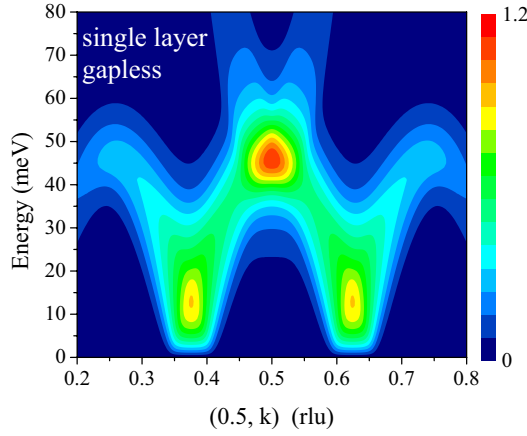


Fig. 3. Plot of the dynamic structure factor $\tilde{S}_{h,k}(\omega)$ in arbitrary units as function of momentum and energy. Note that $\tilde{S}_{h,k}(\omega)$ corresponds to the sum over regions with ladders running in x direction and regions with ladders running in y direction. The parameters apply to LBCO at doping $1/8$,^{5,55} namely $J = 127$ meV, $J_{\text{cyc}}/J = 0.2$ and $J' = -0.072J$. The energy resolution is 6 meV; it is implemented as the imaginary part η in $\omega \rightarrow \omega + i\eta$ in expression (15). The momentum resolution is $\Delta k = 0.03$ rlu which means that at a given momentum (h, k) the weight in the square $(h \pm \Delta k, k \pm \Delta k)$ is averaged. (Color online, gray scale in print version.)

in the structure factor (15). This is so because the matrix element to excite a local triplet depends only on the distance between the two spins on one rung. The phase factor between the layers does not matter.

Finally, we assume that regions with stripes running vertically and regions with stripes running horizontally are equally present in the samples. Hence we will display and discuss the symmetrized data $\tilde{S}_{h,k}(\omega) = (S_{h,k}(\omega) + S_{k,h}(\omega))/2$.

3. Single layer

Results for single layers are presented in our previous work.^{55,56} Very good agreement was obtained for realistic values of the coupling parameters. In particular, it was shown that significant cyclic exchange ($J_{\text{cyc}}/J \approx 0.2$) is needed to reconcile the resonance energy and the global energy scale. In the framework of the stripe model the resonance appears as the saddle point in a strongly anisotropic dispersion.^{54,55} The dispersion is very large along the ladders, i.e. along the stripes, while it is small perpendicular to them. The global energy scale is set by the maximum of the dispersion. It can be determined from the analysis of the dispersion itself⁵⁶ or from the analysis of the momentum-integrated structure factor.⁵⁵

For LBCO at $1/8$ doping, the global energy scale is $J = 127$ meV and the interladder coupling is $J' = -0.072J$. This value corresponds to the quantum critical point where the spin-liquid gap just vanishes. The actual value will be a little larger because there is evidence for (weak) long-range magnetic order.²⁸

Using the single-layer model, the analysis for underdoped YBCO_{6.6} yields $J = 114$ meV and the interladder coupling $J' = -0.035J$.⁵⁶ The significantly smaller value of J' is implied by the presence of a finite spin gap.

A cut through the Brillouin zone is displayed in Fig. 3.

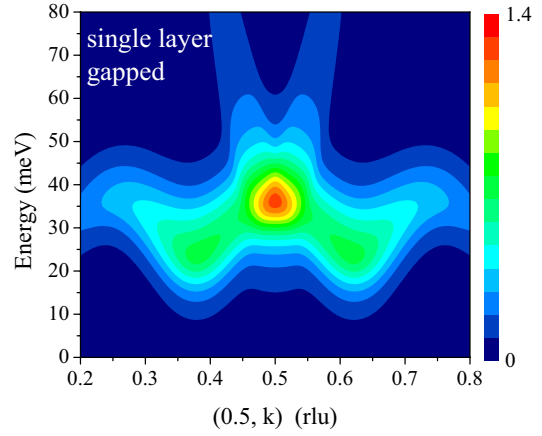


Fig. 4. Plot of the dynamic structure factor $\tilde{S}_{h,k}(\omega)$ in arbitrary units as function of momentum and energy. Based on the single-layer model, the parameters apply to underdoped YBCO_{6.6},^{4,56} namely $J = 114$ meV, $J_{\text{cyc}}/J = 0.2$ and $J' = -0.035J$. The plot is to be compared with Fig. 1i in Ref.⁴ The resolutions are chosen as for Fig. 3. (Color online, gray scale in print version.)

The cut runs parallel to the reciprocal axis through the antiferromagnetic wave vector $\mathbf{Q}_{\text{AF}} = (1/2, 1/2)$. Both the energy dependence and the momentum dependence can be discerned. The values chosen are those which apply to LBCO; finite resolutions in energy and in momentum are taken into account.

Around 45 meV a patch of high intensity at \mathbf{Q}_{AF} is clearly visible. To lower energy the intensity decreases rapidly, becoming significant again at low energies of 10-20 meV. There is finite intensity down to the lowest energies since the system is gapless. It is very remarkable that the finite resolutions lead to the impression of almost vertical rods of high intensity (dark (online: yellow) patches) at the incommensurate positions $(1/2, 1/2 \pm 1/8)$. This coincides nicely with the observations of many experiments, see e.g. the generic graph discussed in Fig. 13b in Ref.¹ We emphasize that the underlying dispersion is sine-shaped as expected, see e.g. Fig. 1 in Ref.⁵⁶

In Fig. 4 the corresponding graph is shown for a gapped system with parameters which apply to underdoped YBCO_{6.6} (Ref.⁴) on the basis of the single-layer model. The theoretical result agrees well with Fig. 1i in Ref.⁴. Clearly, the resonance is dominating and there are tails of intensity to lower energy which point to incommensurate momenta. The intensity toward lower energies is quickly decreasing both in theory and experiment. Discrepancies are seen in the width of the resonance patch which is larger in experiment. It appears also that the shift away from \mathbf{Q}_{AF} is experimentally lower than in our calculation. Since the experimental result is obtained via the subtraction of a background it cannot be excluded that finer features are lost in experiment. Measurements with improved resolution and signal strength will be very interesting to elucidate further details.

4. Bilayer

Now we turn to the properties of bilayer compounds such as YBCO. Before we present results some considerations on the two patterns under study are in order. It

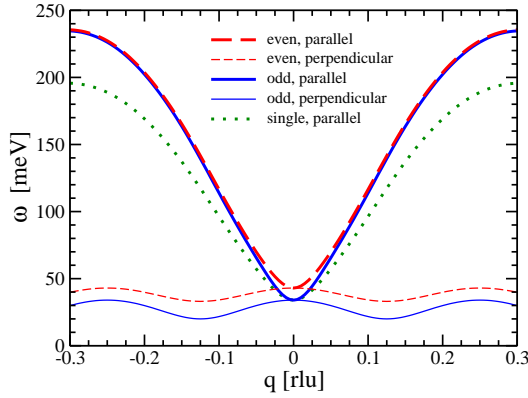


Fig. 5. Dispersion of the odd (solid) and the even (dashed) mode for the in-phase pattern as function of q , the distance to the antiferromagnetic wave vector \mathbf{Q}_{AF} . The thin lines show the dispersion perpendicular to the spin ladders; the thick lines show the dispersion parallel to the spin ladders. The parameters are $J = 136$ meV, $J_s^{\text{ip}} = 0.022J$, $J' = -0.024J$ and $J_{\text{cyc}} = 0.2J$, corresponding to $\Delta = 20$ meV, $\omega_{\text{res}}^{\text{even}} = 43$ meV and $\omega_{\text{res}}^{\text{odd}} = 34$ meV. The dotted line depicts the dispersion in a single layer with $J = 114$ meV, $J' = -0.035J$ and $J_{\text{cyc}} = 0.2J$, corresponding to $\Delta = 20$ meV and $\omega_{\text{res}} = 34$ meV. For these parameters, the dispersion perpendicular to the ladders in the single-layer model (not shown) is indistinguishable from the dispersion of the odd bilayer mode (thin solid line).

is plausible that the out-of-phase pattern is energetically favoured because the charges (the holes in the stripes) are more evenly distributed, see Fig. 2. An even distribution lowers the long-range Coulomb potential. Evidence for such interlayer correlations has been reported on the basis of a hard x-ray diffraction study of Nd-doped LSCO.¹² There, stripes in next-nearest-neighbour layers are found in an out-of-phase arrangement. Note that in this particular case, the nearest-neighbour layers are probably decoupled because the stripes on adjacent layers are running in orthogonal directions due to the coupling to the lattice via the tilting of the oxygen octahedra.

The models for the bilayer have one additional parameter, namely the interlayer coupling. The approximate size of this coupling was discussed above following Eq. (4). We have determined the set of coupling parameters in the following way. We fix the cyclic exchange at the established value of $J_{\text{cyc}}/J = 0.2$ (see above and Refs.^{63,64,67}). The remaining three parameters J , J' and $J_s^{\text{ip/oo}}$ are determined from the experimental values for the spin gap ($\Delta = 20$ meV in YBCO_{6.6}, Ref.⁷⁷) and for the energy of the resonance mode in the odd ($\omega_{\text{res}}^{\text{odd}}$) and in the even channel ($\omega_{\text{res}}^{\text{even}}$). In both channels, the resonance mode corresponds to a saddle point in the two-dimensional, anisotropic dispersion. In underdoped YBCO_{6.6} the odd resonance lies at about $\omega_{\text{res}}^{\text{odd}} = 34$ meV.⁴ Unfortunately, the even resonance has not yet been observed at this doping level. In a slightly overdoped sample, the resonances have been observed at $\omega_{\text{res}}^{\text{even}} = 43$ meV and $\omega_{\text{res}}^{\text{odd}} = 36$ meV.⁷⁸ Since the value of the odd resonance is very similar to the result for YBCO_{6.6}, we assume that also the even resonance is similar and choose $\omega_{\text{res}}^{\text{even}} = 43$ meV and $\omega_{\text{res}}^{\text{odd}} = 34$ meV.

The resulting set of coupling parameters reads $J =$

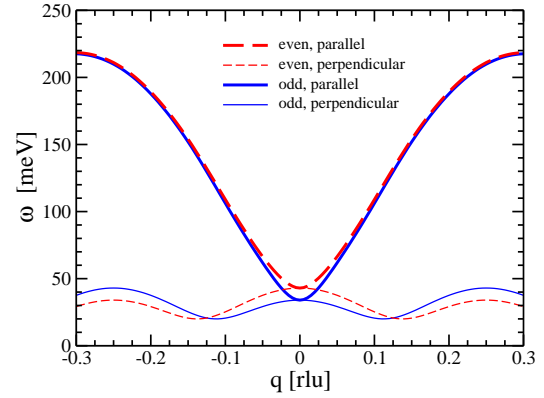


Fig. 6. Dispersion of the odd (solid) and the even (dashed) mode for the out-of-phase pattern as function of q as in Fig. 5. The parameters are $J = 126$ meV, $J_s^{\text{oop}} = -0.026J$, $J' = -0.040J$ and $J_{\text{cyc}} = 0.2J$.

136 meV, $J_s^{\text{ip}} = 0.022J$ and $J' = -0.024J$ for the in-phase pattern and $J = 126$ meV, $J_s^{\text{oop}} = -0.026J$ and $J' = -0.040J$ for the out-of-phase pattern. These two sets will be used in all the plots shown in the following. First, we note that J_s^{ip} is indeed antiferromagnetic and J_s^{oop} is ferromagnetic. Second, the absolute value of J_s^{ip} is fairly small, much smaller than the interlayer coupling in undoped YBCO₆ of $0.08J$. This is another indication that the out-of-phase pattern is more realistic.

Note that J and J' do not change much in the bilayer analyses with respect to the single layer model. The parameter sets all are in an experimentally reasonable range.

In Fig. 5 the dispersions for a single layer and for the bilayer with in-phase pattern are shown. The low-lying dispersion perpendicular to the spin ladders is (almost) the same for the odd mode and for the single layer. This fact corroborates the often made statement that the physics of the odd mode in the bilayer is well described in a model of a single layer. But this does not hold for the dispersion parallel to the spin ladders where the single-layer model implies a significantly lower maximum value. This results from the larger energy scale $J = 136$ meV (instead of 114 meV) needed to meet the resonance energies and the spin gap. The calculated dispersion of the odd mode appears to be steeper than observed experimentally,⁴ but this will have to be clarified by more detailed experiments.

It is striking that the odd and the even mode energies are almost identical above the resonance energies, i.e. above ≈ 50 meV. This can be attributed to the weight factor $a^2(k)$ in Eq. 17, which suppresses the difference between the even and the odd mode for small momenta k (see Fig. 2b in Ref.⁵⁵). At low energies, i.e., $k \approx 0.5$ rlu parallel to the ladders, the coupling between the layers leads to the expected splitting of the two modes.

In Fig. 6, the dispersions for the bilayer with out-of-phase pattern are shown. Again, the odd and the even dispersion almost coincide at energies above the resonances (saddle points). The total dispersion is lower than the one for the in-phase pattern in Fig. 5 but still higher than in the single-layer model.

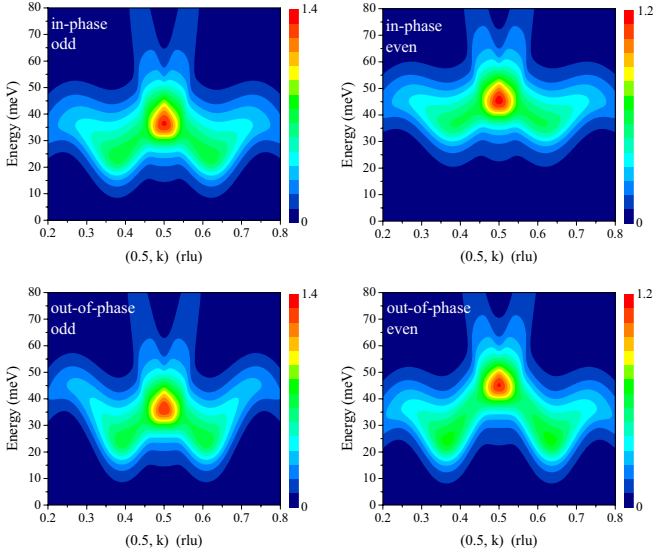


Fig. 7. Plots of the dynamic structure factor $\tilde{S}_{h,k}(\omega)$ (15) for the coupling values as in Figs. 5 and 6. The resolutions in energy and momentum are those used also in Fig. 3. (Color online, gray scale in print version.)

At low energies, the behaviour of the dispersion perpendicular to the ladders is remarkable. It is not just a splitting but the dispersion of one mode can be obtained from the dispersion of the other mode by a translation by $1/4$ rlu perpendicular to the ladders. This is obvious in view of the derivation of the dispersions from the common expression (19). If the dispersion of the even mode can be detected, our predictions in Figs. 5 and 6 will allow to distinguish both correlation patterns clearly. The observation of a splitting at $(1/2, 1/2 \pm 1/8)$ would support the in-phase pattern; the absence of such a splitting would corroborate the out-of-phase scenario. Note that in the out-of-phase pattern *both* modes have the same minimum energy, i.e. the same spin gap.

Another very noteworthy observation concerns the position where the minimum energy is reached. In spite of the underlying commensurate charge modulation, the spin gap is not reached at $q = \pm 1/8$ but at a smaller value (in the odd channel). This results from the sum of the two cosine-terms under the square root in the dispersion (20). Clearly, this effect will be enhanced if J_s^{op} increases relative to J' . It opens up the possibility to vary the incommensurability continuously *without* any change in the periodicity of the charge modulation. This may give rise to a difference in the saturation value of the incommensurability between single layer and bilayer compounds. Such a difference has been discussed in the literature (LSCO:⁹ $\approx 1/8$; YBCO:⁷⁹ $\approx 1/10$). Note, however, that the determination of the incommensurability may be hampered by the asymmetric distribution of the spectral weight (see below).

The Figs. 5 and 6 do not provide information on the intensities. This experimentally crucial information is displayed in Fig. 7. The resonance at \mathbf{Q}_{AF} is dominating in all four plots. The intensity decreases significantly towards lower energies. The response of the odd modes is fairly similar to the response in a single layer (see Fig. 4),

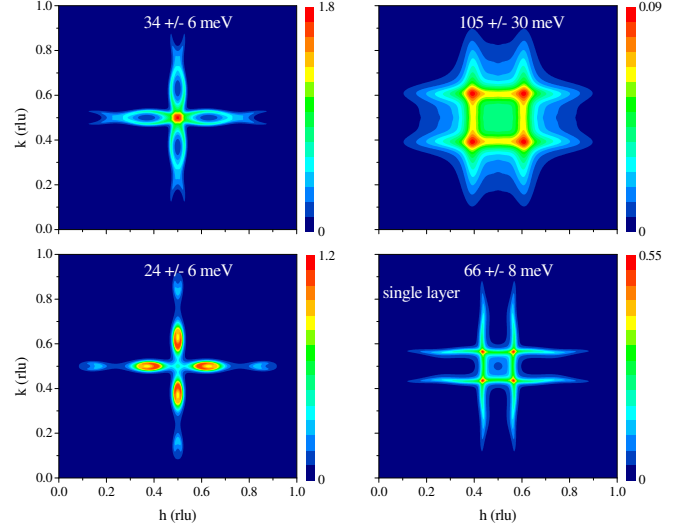


Fig. 8. Constant-energy scans for the single-layer model. The energies and the energy resolutions are given in the figure. There is no broadening in momentum space which must be kept in mind when comparing to experimental data.⁴ The couplings are $J = 114$ meV, $J_{\text{cyc}}/J = 0.2$ and $J' = -0.035J$.⁵⁶ (Color online, gray scale in print version.)

in particular the response for the in-phase pattern. For the out-of-phase pattern, the odd response displays the interesting feature that the resonance is lower in energy than the local maxima of the dispersion at $k = 1/2 \pm 1/4$.

By construction, the resonance of the even modes lies higher in energy. For the in-phase pattern the whole response is located at higher energies than in the odd channel. For the out-of-phase pattern this is not true. There, the intensity of the even mode reaches down to the spin-gap energy of the odd channel. Opposite to the behaviour of the odd dispersion, the local maxima at $k = 1/2 \pm 1/4$ in the even channel are located at lower energies than the even resonance itself.

The results for the odd mode are certainly consistent with the available experimental data. Our spin-only model, however, predicts almost the same intensities for the even and the odd modes. This is at odds with experiment where it seems to be extremely difficult to detect the even mode at all. We presume that the energetically higher lying even modes are affected more strongly by damping effects, for instance due to the eliminated charge degrees of freedom and due to the hard-core triplon-triplon interaction. A strong damping may hinder the experimental observability significantly. This issue certainly calls for further theoretical investigations. However, the damping should be less important at low energies. Thus detailed experimental investigations of the spin gap in the even channel appear very promising.

5. Constant-Energy Scans

The observations made in the previous section are supported by constant-energy scans. For comparison we include in Fig. 8 four scans for a single layer. The energies and the energy resolutions chosen correspond to the experimental ones.⁴ The scan at 24 meV is very close to the spin gap, i.e. the lower bound of the magnetic

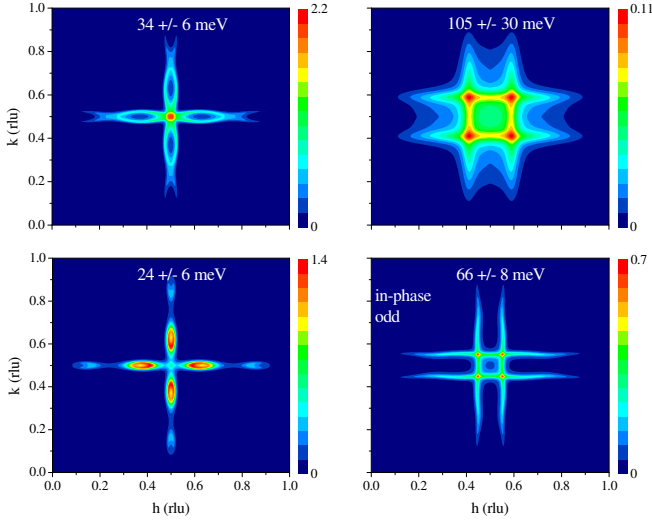


Fig. 9. Constant-energy scans for the odd mode in the in-phase bilayer model. The parameters are $J = 136$ meV, $J_s^{\text{IP}} = 0.022J$, $J' = -0.024J$ and $J_{\text{cyc}} = 0.2J$. (Color online, gray scale in print version.)

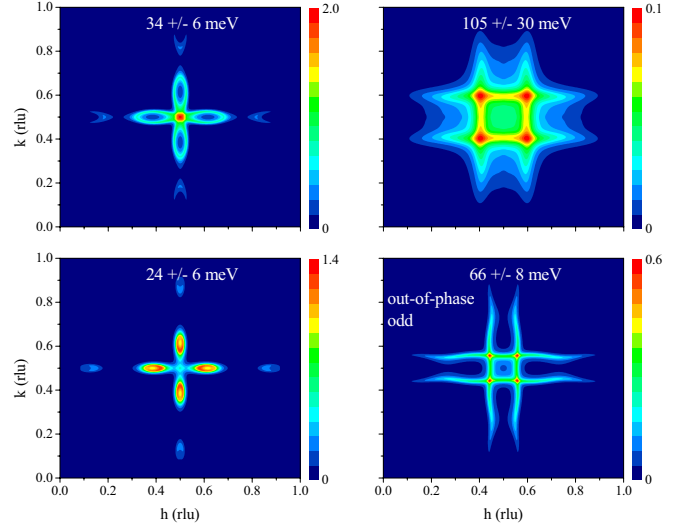


Fig. 11. Constant-energy scans for the odd mode in the out-of-phase bilayer model. The parameters are $J = 126$ meV, $J_s^{\text{OP}} = -0.026J$, $J' = -0.040J$ and $J_{\text{cyc}} = 0.2J$. (Color online, gray scale in print version.)

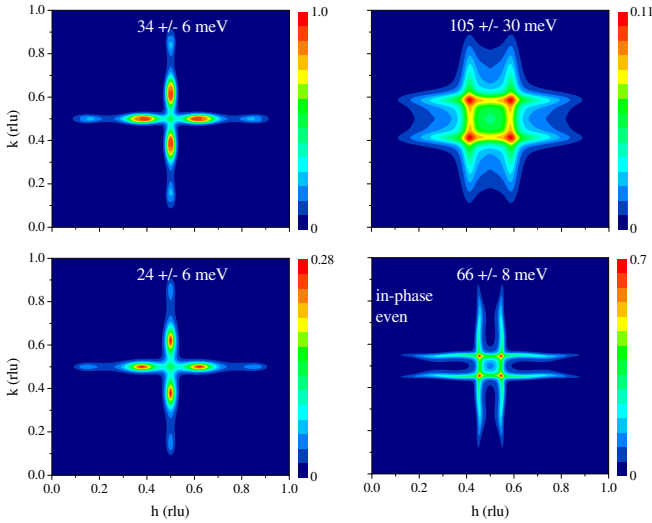


Fig. 10. Constant-energy scans for the even mode in the in-phase bilayer model. Parameters are the same as for Fig. 9. (Color online, gray scale in print version.)

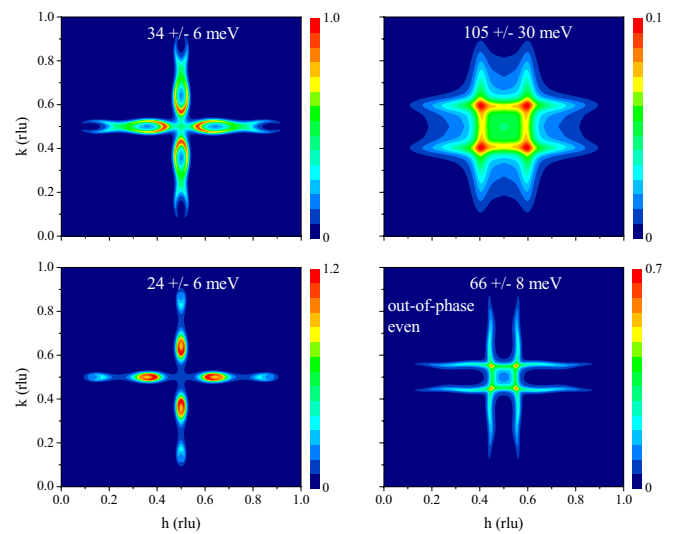


Fig. 12. Constant-energy scans for the even mode in the out-of-phase bilayer model. Parameters are the same as for Fig. 11. (Color online, gray scale in print version.)

excitations. The scan at 34 meV provides data at the resonance energy which corresponds to the saddle point of the dispersion.^{55,56} The two remaining scans provide information at energies above the saddle point.

The theoretical results agree very well with the experimental findings.⁴ In particular, one has a diamond-like shape at low energies of four incommensurate satellites which merge at the resonance energy to an almost circular single patch at \mathbf{Q}_{AF} . Note that already at 24 meV the peak intensity has shifted towards \mathbf{Q}_{AF} , which may blur the precise value of the incommensurability in the analysis of experimental data. Above the resonance energy the shape is square-like with maxima of the intensity at the corners. The theoretical result at higher energies displays a very low intensity at \mathbf{Q}_{AF} while the experiment

shows squares with non-negligible intensity inside. Furthermore, the tails of intensity outside the squares are only very vaguely seen in experiment. We attribute both features to multi-triplon contributions and life-time effects⁵⁵ which we neglected in our approach. But in view of the simplicity of the model, the agreement obtained is remarkable.

In Fig. 9 the same scans are depicted for the odd triplon in the in-phase pattern. Qualitatively, these plots are identical to the ones for the single layer in Fig. 8. At low energies this is even true on a quantitative level which can be taken as an argument that a single-layer calculation captures a significant portion of the physics of the odd modes in a bilayer system. At higher energies, however, the structures are narrower (i.e. closer to \mathbf{Q}_{AF})

in the bilayer due to the larger value of J , as mentioned in the discussion of the dispersion shown in Fig. 5.

In Fig. 10 the scans for the even mode are shown. At high energies they are almost identical to those for the odd mode in Fig. 9. The most striking differences occur at low energies where the intensities are much lower. Note that the scan at 24 meV runs *below* the spin gap of the even mode, the finite intensity is caused only by the broadening. The scans for the odd and the even mode at 34 meV differ decisively because only in the former case the saddle point is hit. This explains the differences in shape and in maximum intensity.

The results for the out-of-phase pattern are presented in Figs. 11 and 12. Again, the odd and the even response are almost identical at high energies while they differ at lower energies. The most striking difference is whether the resonant saddle point is hit (at 34 meV for the odd mode) or not (at 34 meV for the even mode). Very interesting is the situation at 24 meV. In the in-phase pattern (see Figs. 9 and 10) the even mode and the odd mode yield the same shape but the intensity differs by a factor of 5. In the out-of-phase pattern there is no significant difference in the intensities between the odd and the even result. But a closer look reveals that the diamond in the odd channel is smaller than the one in the even channel (see also the dispersion in Fig. 6). This results from the fact that in spite of the given charge modulation the position of the minima depends on the ratio of the prefactors of the two cosine-terms in the dispersion (20), in particular on the sign of this ratio. For ferromagnetic $J_s^{\text{oop}} < 0$ the minima in the odd channel are closer to \mathbf{Q}_{AF} than without interlayer coupling while the minima in the even channel are further away from \mathbf{Q}_{AF} . These low energy features should be robust against the damping by charge degrees of freedom and thus appear as promising candidates for future experiments.

6. Conclusions

We investigated a spin-only model with stripe order in a single layer and for two patterns in a bilayer. In the first pattern, the stripes and hence the spin ladders are *in-phase* in the two layers; in the second pattern they are arranged *out-of-phase*, see Fig. 2. The patterns are taken to be long-range in our calculation. But for systems like YBCO we view the assumption of long-range stripe order as an approximation to fluctuating medium-range correlations. This approximation significantly eases the theoretical treatment.

The calculation was done by coupling the effective model, which was obtained previously for isolated spin ladders with cyclic exchange by continuous unitary transformations. The effective model is formulated in terms of triplons, the elementary triplet excitations. The coupling *between* the ladders is small so that the neglect of the hard-core constraint of the triplons is justified. Thereby, we can obtain quantitative results.

The results obtained within the single-layer model agree very well with experimental findings, both for gapless^{5,55} and for gapped systems.^{4,56} We stress that the coupling parameters J and J_{cyc} are realistic ones and that only one parameter (J') has not been derived inde-

pendently from other experiments. In the gapless case we have shown that the finite resolution in momentum and energy leads to the impression of almost vertical rods in the (ω, k) plane (Fig. 3), very much like what is seen in many experiments. In the gapped phase, our calculation reproduces the experimentally observed rapid decrease of intensity towards lower energies.

In the bilayer system we distinguish contributions from the odd and from the even triplon mode. Independent of the stripe pattern considered the result in the odd channel resembles very much what is obtained for a single layer. This finding confirms the often used assumption that a model with a single layer suffices to capture the physics in the odd channel of the bilayer system. The agreement between odd channel and single-layer results is almost quantitative for the in-phase stripe correlations, at least at low energies. For the out-of-phase pattern, the odd mode dispersion does not have its minimum at $(1/2, 1/2 \pm \delta)$ with $\delta = 1/8$, but at smaller values $\delta < 1/8$. So we have discovered a way to reconcile values of δ different from $1/8$ with a charge correlation dominated by the periodicity $4a$.

The even modes behave almost quantitatively like the odd modes at energies higher than the resonance energies. At energies of the order of the resonance energies the even and odd modes split. In the in-phase pattern this splitting does not depend on the momentum h perpendicular to the ladders. In the out-of-phase pattern, however, the even mode dispersion and the odd mode dispersion can be derived from each other by a translation by $1/4$ rlu perpendicular to the stripes. This implies that both modes have the same spin gap, that means the intensity of the even modes reaches also down to low energies. Furthermore, we predict that the even mode displays a larger shift in the position of its minima located at $(1/2, 1/2 \pm \delta)$ with $\delta > 1/8$. These predictions can be tested experimentally if the even mode can be observed.

One serious discrepancy between theory and experiment arises from the relative intensities of the even and the odd modes. The even mode is hardly seen in experiment. So far it is only seen in the undoped parent compound YBCO₆^{68,69} and in a slightly overdoped, Ca substituted sample Y_{0.9}Ca_{0.1}Ba₂Cu₃O₇.⁷⁸ In the latter sample the intensity is reduced by a factor of 3 with respect to the odd mode whereas our calculation implies that the reduction in intensity should only be about 20%. This discrepancy can possibly be attributed to the stronger damping that the even mode experiences because it lies at higher energy. A significant damping broadens the response so that it becomes difficult to distinguish from the omnipresent backgrounds, thus the signal is lost. The damping might be due to (i) the eliminated charge degrees of freedom, (ii) the hard-core interaction between the triplons or (iii) multi-triplon contributions. The issue which processes are the important ones must be left to future research.

In this context one may also speculate about a possible doping dependence of $\omega_{\text{res}}^{\text{even}}$. Experimentally, it has been established that the *odd* resonance shifts to lower energies with decreasing doping.³ Assuming that this shift

is at least partly caused by an increase of the modulus of the interlayer coupling $J_s^{\text{ip/ooP}}$, it corresponds to an increase of $\omega_{\text{res}}^{\text{even}}$ with decreasing doping, and thus also to an increased damping of the even mode.

We advocate the out-of-phase pattern as the more likely candidate to describe the relevant bilayer correlations. First, the concomitant charge distribution is more even, so the Coulomb interaction favours the out-of-phase pattern. Second, the small value of the interlayer coupling of about 2-3% of J (compared to 8% in the undoped parent compound) is indicative that it is not the direct exchange from one layer to the other as in Fig. 2a which is responsible for the interlayer coupling. For the out-of-phase pattern shown in Fig. 2b it is natural to assume that the (absolute) value of J_s^{op} is small. Third, it is appealing to attribute values of the incommensurability different from $1/8$ to the tunable incommensurability in the out-of-phase pattern.

It is remarkable to which extent the straightforward model of coupled spin ladders describes the emerging universal behaviour of the magnetic excitations in high-temperature superconducting cuprates. This is even more fascinating in view of the fact that static stripes are not supported by experiment³⁷ and of the tendency to form more two-dimensional tiling patterns, at least at the surfaces.^{44,80} We think that the universal behaviour of the magnetic excitations may be explained by assuming that on a medium-range of 4 to 8 lattice spacings the correlations are similar to those of stripes. It is plausible that our results for not too low energies remain qualitatively valid for such a system with medium-range stripe correlations. Definitely, more work is called for to improve the theoretical description further.

Equally, further high-resolution neutron experiments are desirable in order to test the predictions made in the present work. This will provide deeper insight in the complex physics of the elementary excitations of the cuprate superconductors.

Acknowledgment

Helpful discussions are acknowledged with M. Braden, B. Keimer, S. Sachdev, J.M. Tranquada, M. Vojta and T. Yokoo. This work was supported by the DFG in SFB 608 and in SP 1073 as well as by the COE at the Tohoku University, Sendai, where a part of this work was done during a visiting professorship of one of us (GSU).

- 1) H. B. Brom and J. Zaanen, in *Handbook of Magnetic Materials*, by K. H. J. Buschow, vol. 15, p. 379 (Elsevier, New York, 2003)
- 2) M. R. Norman and C. Pépin, Rep. Prog. Phys. **66** (2003) 1547.
- 3) Y. Sidis, S. Pailhès, B. Keimer, P. Bourges, C. Ulrich and L. P. Regnault, phys. stat. sol. **241** (2004) 1204.
- 4) S. M. Hayden, H. A. Mook, P. Dai, T. G. Perring and F. Doğan, Nature **429** (2004) 531.
- 5) J. M. Tranquada, H. Woo, T. G. Perring, H. Goka, G. D. Gu, G. Xu, M. Fujita and K. Yamada, Nature **429** (2004) 534.
- 6) N. B. Christensen, D. F. McMorro, H. M. Ronnow, B. Lake, S. M. Hayden, G. Aeppli, T. G. Perring, M. Mangkorntong, M. Nohara and H. Tagaki, cond-mat/0403439.
- 7) S. Wakimoto, G. Shirane, Y. Endoh, K. Hirota, S. Ueki, K. Yamada, R. J. Birgeneau, M. A. Kastner, Y. S. Lee, P. M. Gehring

- and S. H. Lee, Phys. Rev. B **60** (1999) R769.
- 8) M. Fujita, K. Yamada, H. Hiraka, P. M. Gehring, S. H. Lee, S. Wakimoto and G. Shirane, Phys. Rev. B **65** (2002) 064505.
- 9) K. Yamada, C. H. Lee, K. Kurahashi, J. Wada, S. Wakimoto, S. Ueki, H. Kimura, Y. Endoh, S. Hosoya, G. Shirane, R. J. Birgeneau, M. Greven, M. A. Kastner and Y. J. Kim, Phys. Rev. B **57** (1998) 6165.
- 10) A. H. Castro Neto and C. Morais Smith, cond-mat/0304094.
- 11) J. M. Tranquada, B. J. Sternlieb, J. D. Axe, Y. Nakamura and S. Uchida, Nature **375** (1995) 561.
- 12) M. v. Zimmermann, A. Vigliante, T. Niemöller, N. Ichikawa, T. Frello, J. Madsen, P. Wochner, S. Uchida, N. H. Andersen, J. M. Tranquada, D. Gibbs and J. R. Schneider, Europhys. Lett. **41** (1998) 629.
- 13) S.-W. Cheong, G. Aeppli, T. E. Mason, H. Mook, S. M. Hayden, P. C. Canfield, Z. Fisk, K. N. Clausen and J. L. Martinez, Phys. Rev. Lett. **67** (1991) 1791.
- 14) T. E. Mason, A. Schröder, G. Aeppli, H. A. Mook and S. M. Hayden, Phys. Rev. Lett. **77** (1996) 1604.
- 15) G. Aeppli, S. M. Hayden, P. Dai, H. A. Mook, R. D. Hung, T. G. Perring and F. Dogan, Science **278** (1997) 1432.
- 16) B. Lake, G. Aeppli, T. E. Mason, A. Schröder, D. F. McMorro, K. Lefmann, M. Isshiki, M. Nohara, H. Takagi and S. M. Hayden, Nature **400** (1999) 43.
- 17) H. Hiraka, Y. Endoh, M. Fujita, Y. S. Lee, J. Kulda, A. Ivanov and R. J. Birgeneau, J. Phys. Soc. Jpn. **70** (2001) 853.
- 18) J. M. Tranquada, C. H. Lee, K. Yamada, Y. S. Lee, L. P. Regnault and H. M. Ronnow, Phys. Rev. B **69** (2004) 174507.
- 19) J. Rossat-Mignot, L. P. Regnault, C. Vettier, P. Bourges, P. Burlet, J. Bossy, J. Y. Henry and G. Lapertot, Physica **C185-189** (1991) 86.
- 20) H. He, P. Bourges, Y. Sidis, C. Ulrich, L. P. Regnault, S. Pailhès, N. S. Berzigiarova, N. N. Kolesnikov and B. Keimer, Science **295** (2002) 1045.
- 21) M. Arai, T. Nishijima, Y. Endoh, T. Egami, S. Tajima, K. Tomimoto, Y. Shiohara, M. Takahashi, A. Garrett and S. M. Bennington, Phys. Rev. Lett. **83** (1999) 608.
- 22) P. Bourges, Y. Sidis, H. F. Fong, L. P. Regnault, J. Bossy, A. Ivanov and B. Keimer, Science **288** (2000) 1234.
- 23) D. Reznik, P. Bourges, L. Pintschovius, Y. Endoh, Y. Sidis, Y. Shiokara and S. Tajima, Phys. Rev. Lett. **93** (2004) 207003.
- 24) T. Yokoo, M. Arai, Y. Shiohara, S. Tajima, C. D. Frost and Y. Endoh, Physica **C388** (2003) 223.
- 25) T. Yokoo, M. Arai, Y. Shiohara, S. Tajima, C. D. Frost and Y. Endoh, J. Low Temp. Phys. **131** (2003) 731.
- 26) H. A. Mook, P. C. Dai and F. Dogan, Phys. Rev. Lett. **88** (2002) 097004.
- 27) A. R. Moodenbaugh, Y. Xu, M. Suenaga, T. J. Folkerts and R. N. Shelton, Phys. Rev. B **38** (1988) 4596.
- 28) M. Fujita, H. Goka, K. Yamada, J. M. Tranquada and L. P. Regnault, Phys. Rev. B **70** (2004) 104517.
- 29) D. K. Morr and D. Pines, Phys. Rev. Lett. **81** (1998) 1086.
- 30) A. Abanov and A. V. Chubukov, Phys. Rev. Lett. **83** (1999) 1652.
- 31) H. J. Schulz, J. Phys. I France **50** (1989) 2833.
- 32) J. Zaanen and O. Gunnarsson, Phys. Rev. B **40** (1989) 7391.
- 33) C. H. Chen, S.-W. Cheong and A. S. Cooper, Phys. Rev. Lett. **71** (1993) 2461.
- 34) J. M. Tranquada, D. J. Buttrey, V. Sachan and J. E. Lorenzo, Phys. Rev. Lett. **73** (1994) 1003.
- 35) H.-H. Klauss, W. Wagener, M. Hillberg, W. Koopmann, H. Walf, F. J. Litterst, M. Hücker and B. Büchner, Phys. Rev. Lett. **85** (2000) 4590.
- 36) L. Balents, L. Bartosch, A. Burkov, S. Sachdev and K. Sengupta, cond-mat/0409470.
- 37) V. Hinkov, S. Pailhès, P. Bourges, Y. Sidis, A. Ivanov, A. Kulakov, C.T. Lin, D.P. Chen, C. Bernhard and B. Keimer, Nature **430** (2004) 650.
- 38) V. J. Emery, S. A. Kivelson and O. Zachar, Phys. Rev. B **56** (1997) 6120.
- 39) S. A. Kivelson, I. P. Bindloss, E. Fradkin, V. Oganessian, J. M. Tranquada, A. Kapitulnik and C. Howald, Rev. Mod. Phys. **75** (2003) 1201.

- 40) V. I. Anisimov, M.A. Korotin, A.S. Mylnikova, A.V. Kozhevnikov and J. Lorenzana, *cond-mat/0402162*.
- 41) H. J. Schulz, *Phys. Rev. B* **34** (1986) 6372.
- 42) E. Dagotto and T. M. Rice, *Science* **271** (1996) 618.
- 43) J. Tworzydło, O. Y. Osman, C. N. A. van Duin and J. Zaanen, *Phys. Rev. B* **59** (1999) 115.
- 44) T. Hanaguri, C. Lupien, Y. Kohsaka, D.-H. Lee, M. Azuma, M. Takano, H. Takagi and J. C. Davis, *Nature* **430** (2004) 1001.
- 45) A. P. Schnyder, A. Bill, C. Mudry, R. Gilardi, H. M. Rønnow and J. Mesot, *Phys. Rev. B* **70** (2004) 214511.
- 46) D. Zanchi and H. J. Schulz, *Phys. Rev. B* **61** (2000) 13609.
- 47) N. Furukawa, C. Honerkamp, M. Salmhofer and T. M. Rice, *Physica B* **284** (2000) 1575.
- 48) C. J. Halboth and W. Metzner, *Phys. Rev. B* **61** (2000) 7364.
- 49) A. Abanov, A. V. Chubukov and J. Schmalian, *Adv. Phys.* **52** (2003) 119.
- 50) S. Schmitt-Rink, C. M. Varma and A. E. Ruckenstein, *Phys. Rev. Lett.* **60** (1988) 2793.
- 51) E. Dagotto, *Rev. Mod. Phys.* **66** (1994) 763.
- 52) E. Demler, W. Hanke and S.-C. Zhang, *Rev. Mod. Phys.* **76** (2004) 909.
- 53) L. Balents, L. Bartosch, A. Burkov, S. Sachdev and K. Sengupta, *cond-mat/0408329*.
- 54) M. Vojta and T. Ulbricht, *Phys. Rev. Lett.* **93** (2004) 127002.
- 55) G. S. Uhrig, K. P. Schmidt and M. Grüninger, *Phys. Rev. Lett.* **93** (2004) 267003.
- 56) G. S. Uhrig, K. P. Schmidt and M. Grüninger, *J. Mag. Mag. Mat. in press* (2005)
- 57) M. Vojta and S. Sachdev, *cond-mat/0408461*.
- 58) G. Seibold and J. Lorenzana, *cond-mat/0406589*.
- 59) H. J. Schmidt and Y. Kuramoto, *Physica B* **163** (1990) 443.
- 60) E. Müller-Hartmann and A. Reischl, *Eur. Phys. J. B* **28** (2002) 173.
- 61) A. Reischl, E. Müller-Hartmann and G. S. Uhrig, *Phys. Rev. B* **70** (2004) 245124.
- 62) J. Lorenzana, J. Eroles and S. Sorella, *Phys. Rev. Lett.* **83** (1999) 5122.
- 63) R. Coldea, S. M. Hayden, G. Aeppli, T. G. Perring, C. D. Frost, T. E. Mason, S. W. Cheong and Z. Fisk, *Phys. Rev. Lett.* **86** (2001) 5377.
- 64) A. A. Katanin and A. P. Kampf, *Phys. Rev. B* **66** (2002) 100403.
- 65) M. Matsuda, K. Katsumata, R. S. Eccleston, S. Brehmer and H.-J. Mikeska, *Phys. Rev. B* **62** (2000) 8903.
- 66) M. Windt, M. Grüninger, T. Nunner, C. Knetter, K. Schmidt, G. S. Uhrig, T. Kopp, A. Freimuth, U. Ammerahl, B. Büchner and A. Revcolevschi, *Phys. Rev. Lett.* **87** (2001) 127002.
- 67) T. Nunner, P. Brune, T. Kopp, M. Windt and M. Grüninger, *Phys. Rev. B* **66** (2002) 180404.
- 68) D. Reznik, P. Bourges, H. F. Fong, L. P. Regnault, J. Bossy, C. Vettier, D. L. Milius and I. A. Aksay, *Phys. Rev. B* **53** (1996) R14741.
- 69) S. M. Hayden, G. Aeppli, T. G. Perring, H. A. Mook and F. Dogan, *Phys. Rev. B* **54** (1996) R6905.
- 70) M. Grüninger, D. van der Marel, A. Damascelli, A. Erb, T. Nunner and T. Kopp, *Phys. Rev. B* **62** (2000) 12422.
- 71) C. Knetter, K. P. Schmidt, M. Grüninger and G. S. Uhrig, *Phys. Rev. Lett.* **87** (2001) 167204.
- 72) K. P. Schmidt, H. Monien and G. S. Uhrig, *Phys. Rev. B* **67** (2003) 184413.
- 73) K. P. Schmidt and G. S. Uhrig, *Phys. Rev. Lett.* **90** (2003) 227204.
- 74) T. Barnes, E. Dagotto, J. Riera and E. S. Swanson, *Phys. Rev. B* **47** (1993) 3196.
- 75) T. Barnes and J. Riera, *Phys. Rev. B* **50** (1994) 6817.
- 76) S. Trebst, H. Monien, C. J. Hamer, Z. Weihong and R.R.P. Singh, *Phys. Rev. Lett.* **85** (2000) 4373.
- 77) P. Dai, H. A. Mook, S. M. Hayden, G. Aeppli, T. G. Perring, R. D. Hunt and F. Dogan, *Science* **285** (1999) 1344.
- 78) S. Pailhès, Y. Sidis, P. Bourges, C. Ulrich, V. Hinkov, L. P. Regnault, A. Ivanov, B. Liang, C. T. Lin, C. Bernhard and B. Keimer, *Phys. Rev. Lett.* **91** (2003) 237002.
- 79) P. Dai, H. A. Mook, R. D. Hunt and F. Dogan, *Phys. Rev. B* **63** (2001) 054525.
- 80) K. McElroy, D.H. Lee, J. E. Hoffman, K. M. Lang, J. Lee, E. W. Hudson, H. Eisaki, S. Uchida and J. C. Davis, *cond-mat/0406491*.

Magnetic Excitations in Bilayer High-Temperature Superconductors with Stripe Correlations

G.S. UHRIG^{1*}, K.P. SCHMIDT¹ and M. GRÜNINGER²

¹*Institut für Theoretische Physik, Zülpicher Straße 77, Universität zu Köln, 50937 Köln, Germany*

²*Physikalisches Institut, RWTH Aachen, 52056 Aachen, Germany*

The universal behaviour of the magnetic excitations in high-temperature superconductors is described in a model with static stripes retaining only the localized spin degrees of freedom. The stripes are represented by a model of coupled two-leg spin ladders. We start from the results obtained previously by continuous unitary transformations for an isolated spin ladder. A quantitative description of neutron scattering data is reached, using a model for a single cuprate layer with well established values of the exchange coupling constants. The neutron resonance peak is explained in terms of a saddle point in the dispersion of the magnetic excitations. Here we make predictions for bilayer systems with in-phase or out-of-phase stripe correlations. The results may serve as a guide for future experimental analyses.

KEYWORDS: magnetic excitations, spectral densities, stripe phase, inelastic neutron scattering, high-temperature superconductors

1. Introduction

The rôle of the magnetic excitations in the mechanism of high-temperature superconductivity is still heavily debated. A prerequisite for a successful understanding of this rôle is a quantitative description of the magnetic excitations themselves. For many years, however, it seemed that different families of compounds display rather different behaviour of their magnetic excitations.^{1–3} Recent experimental evidence for a universal behaviour of the magnetic excitations^{4–6} clearly indicates the relevance of these features and calls for detailed theoretical investigations.

Phenomena In the single-layer compound $\text{La}_{2-x}\text{Sr}_x\text{CuO}_4$ (LSCO), four incommensurate satellites are observed in elastic neutron scattering experiments at low temperatures. These satellites are shifted away from the antiferromagnetic wave vector $\mathbf{Q}_{\text{AF}} = (1/2, 1/2)$ in reciprocal lattice units (rlu). In the insulating phase at low doping ($p \lesssim 6\%$), the shift occurs along the diagonal while it occurs parallel to the tetragonal reciprocal axes in the superconducting phase ($p \gtrsim 6\%$).^{7,8} The size of the shift is roughly linear in the doping p for small values of p . It saturates at about $1/8$ of the Brillouin zone for sizeable doping levels ($p \gtrsim 10\%$),^{8,9} see also Fig. 1.4 in Ref.¹⁰ These incommensurate features may be explained in terms of the superstructure satellites of a stripe phase (see below), which is supported by the observation of the corresponding charge-order satellites around the Bragg peaks in Nd-doped LSCO.^{11,12} Incommensurate magnetic excitations were observed in LSCO also in *inelastic* neutron scattering (INS) experiments.^{6,13–18}

In the bilayer compound $\text{YBa}_2\text{Cu}_3\text{O}_x$ (YBCO_x), the magnetic response at optimum doping is dominated below T_c by the resonance peak at \mathbf{Q}_{AF} with an energy of $\omega_{\text{res}} \approx 41$ meV.^{1,3,19} The observation of a resonance peak at \mathbf{Q}_{AF} below T_c with $\omega_{\text{res}} \approx 47$ meV in single layer $\text{Ti}_2\text{Ba}_2\text{CuO}_y$ ²⁰ shows that the bilayer structure is not a

prerequisite for the occurrence of the resonance peak. Incommensurate branches have been observed at low energies in the underdoped regime and more recently also at about optimal doping.^{21–25} Elastic superstructure satellites indicating charge order were also reported in underdoped YBCO,²⁶ suggesting that also this system may display an instability towards stripe formation. A third feature is the appearance of incommensurate branches *above* the resonance energy.^{21,23–26}

Universality The data for YBCO provide evidence that the resonance peak and the incommensurate excitations are not separate features but form part of the common dispersive magnetic excitations of the cuprate high-temperature superconductors. Very recently, this point of view has been substantiated by reports on very similar INS data obtained on $\text{YBCO}_{6.6}$ ⁴ and $\text{La}_{15/8}\text{Ba}_{1/8}\text{CuO}_4$ (LBCO),⁵ both at low and at high energies in a large part of the Brillouin zone. On the one hand, the experiment of Tranquada and co-workers on LBCO⁵ provides data for a *charge-ordered* phase which suppresses the superconducting phase.^{27,28} The data show the incommensurate excitations which are familiar in the La family. Additionally, a dominant feature is observed at \mathbf{Q}_{AF} , which is the first report of such a resonance in this family. In contrast to YBCO, the resonance in LBCO is observed in the normal (charge-ordered) state. On the other hand, the experiment by Hayden and co-workers for $\text{YBCO}_{6.6}$ displays very similar features.⁴ Yet the system is in the *superconducting* state. Recently, Christensen *et al.* pointed out the similarity of the dispersion in the superconducting phases of optimally doped LSCO and YBCO.⁶

These findings suggest that the magnetic excitations in the high- T_c cuprate superconductors are of universal character. Differences may stem from the differences in the state of the charges. The absence of a resonance peak in LSCO may be explained by the position of the resonance mode with respect to the particle-hole continuum. If the decay into particle-hole pairs is fast the magnetic

*E-mail address: gu@thp.uni-koeln.de

modes may be overdamped so that they are not seen in experiment as prominent peaks.^{29,30} In fact, the incommensurate magnetic excitations in LSCO become much sharper upon cooling.^{14,15}

Modulated Phases An appealing route to account for the important features of the magnetic excitations sketched above is to assume a certain long-range charge modulation. This implies a corresponding superstructure in the spin sector which in turn leads to periodicities different from those of the underlying lattice. The most prominent modulation considered is the formation of stripes. It was proposed theoretically in the late eighties^{31,32} on the basis of the energy gain due to binding of charges to domain walls. Later such modulations were observed experimentally in, e.g., nickelates,^{33,34} and cuprates.¹¹

While there are certain cuprate systems for which the existence of static stripes is well established, e.g., rare-earth-doped LSCO,^{11,12,35} there are others which do not appear to display static long-range stripes, for instance optimally doped YBCO. We like to emphasize, however, that there are theoretical predictions based on phenomenological dimer models which show that even very small charge modulations can have a sizeable effect on the spin sector, e.g., inducing a significant modulation of dimer correlations.³⁶ So it is not excluded that certain charge orderings eluded so far experimental observation because of their smallness.

Recent experiments on an *untwinned* sample of slightly underdoped YBCO_{6.85}³⁷ have not found a significant anisotropy in the weights of the incommensurate peaks. The data display a certain anisotropy regarding the peak width. Assuming that a given orthorhombic domain determines the orientation of a possible stripe order these findings do not support the existence of a static one-dimensional stripe pattern, but they may be consistent with fluctuating stripes. For a further discussion of the physics of static or dynamic stripes we refer to Refs.^{1,10,38,39}

Stripe Pattern The stripe phase corresponds to a segregation into hole-rich and hole-poor ribbons. Experimentally, a doping dependence of the periodicity has been reported in elastic neutron scattering experiments on underdoped LSCO.^{8,9} The shift of the magnetic satellites away from \mathbf{Q}_{AF} saturates at about $1/8$ for larger doping levels ($p \approx 0.1$), see e.g. Fig. 1.4 in Ref.,¹⁰ corresponding to a spin superstructure periodicity of $8a$ where a is the in-plane lattice constant. The concomitant charge superstructure periodicity of static stripes is found to be $4a$.^{11,12} This is the periodicity we choose in our model. The spin superstructure of $8a$ can be explained by, e.g., assuming that the hole-rich ribbons form anti-phase domain walls for the spins, corresponding to an effective *ferromagnetic* coupling between the spins across a hole-rich stripe (see below).

In the literature, two patterns of stripe modulation are studied. One is the site-centered pattern where the hole-rich stripe is a chain, i.e. the width of this stripe is only one site. Neighbouring hole-rich stripes are separated by three hole-poor sites with localized spins, which can be viewed as a three-leg spin ladder. This pattern

is the one that was considered mostly.¹ But an attractive alternative is the bond-centered pattern where the hole-rich stripe has a width of two sites. These stripes are separated by two hole-poor spin sites, corresponding to a two-leg spin ladder (see Fig. 1). There is evidence from band structure calculations that the bond-centered modulation is favourable.⁴⁰ Moreover, the magnetic state is more stable in the bond-centered pattern than in the site-centered one because spin ladders with an even number of legs are gapped^{41,42} and thus stable against small perturbations. Spin ladders with odd number of legs are critical^{41,42} and thus highly unstable against any perturbation or spontaneous symmetry breaking. A quantum Monte-Carlo study illustrates that in the bond-centered pattern much of the fluctuations originate directly in the spin sector while in the site-centered pattern the interplay between spin and charge sector is essential.⁴³

Another interesting piece of evidence in favour of the bond-centered scenario can be derived from the Fourier analysis of the modulations observed by scanning tunneling microscopy (STM)⁴⁴ on underdoped $\text{Ca}_{2-x}\text{Na}_x\text{CuO}_2\text{Cl}_2$. We interpret the data here as resulting from the spatial average of vertical and horizontal stripes. A discussion of a possible truly two-dimensional 4×4 tiling modulation is left to future research. The STM data show features at $\pm 1/4$ rlu, but not at $1/2$ rlu. The bond-centered modulation with period $4a$ is indeed generated by a single cosine term with wave vector $2\pi/4a$; no higher harmonics appear. In contrast, the general site-centered modulation with period $4a$ is characterized by the fundamental and the first harmonic. Hence, the generic site-centered modulation should display a feature also at $1/2$ rlu. Thus the STM data rather support the bond-centered scenario.

Theoretical Approaches There are many theoretical approaches to the magnetic excitations in the cuprate superconductors.² They can be split into two classes:

(i) Starting from an underlying *fermionic* model, mostly extended Hubbard models, one has to deal with strong interactions. The magnetic collective modes appear in the particle-hole or particle-particle channel. In essence, they are bound states or resonances of two fermions.² Widely used techniques in this field are approaches based on random phase approximations (see e.g. Ref.⁴⁵ and references therein), and renormalization schemes (see e.g. Refs.⁴⁶⁻⁴⁸). The regime of strong interactions with coupling constants larger than the band width is difficult to describe reliably.

(ii) Alternatively, one may start from a bosonic model which contains the collective modes already from the very beginning. Then the interplay with the charge degrees of freedom is added by some coupling. The approaches based on spin-fermion models^{29,49} or many treatments of t - J models^{50,51} are of this type. In the very limit, the fermionic excitations are neglected, focusing on the collective modes alone (see e.g. Refs.^{52,53}).

In the present work we use an approach of the second type. We discuss a spin-only Heisenberg model of coupled spin ladders with effective coupling parameters, assuming that the charge degrees of freedom are integrated out. Roughly speaking, the excitation energies of

the charge degrees of freedom are of the order of t while the magnetic energies are of the order of $J \approx t/3$. So it makes sense to consider an effective magnetic model at low energies with the faster charge degrees of freedom being eliminated. One has to keep in mind that the decay of the magnetic collective modes into particle-hole pairs is neglected which will certainly play a rôle at higher energies. Neglecting this decay is well justified in the superconducting state where the charge excitations are mostly gapped.

While we start from a spin-only model with long-range stripe order our predictions are equally relevant for systems with fluctuating stripe order for not too low energies. The time scale of these fluctuations should be above the time scale set by the inverse energy of the features under study.

Vojta and Ulbricht⁵⁴ investigated the same spin-only model without the cyclic spin exchange (see below) by a mean-field approach starting from dimers on the rungs of the ladders. The description of isolated ladders is improved by a local energy correction which accounts for a part of the effect of the hard-core constraint of the excitations on each dimer. The constant-energy scans in this approach agree qualitatively with the results we obtained for a single-layer model.^{55,56}

In a phenomenological approach Vojta and Sachdev considered also a plaquette modulation.⁵⁷ From their results they concluded that the magnetic excitations of a plaquette modulation do not agree with the inelastic neutron data.^{4,5}

Seibold and Lorenzana performed a large-scale time-dependent Gutzwiller calculation for a Hubbard model to determine the magnetic excitations of a stripe phase with charge and spin order.⁵⁸ Using parameters adapted to describe the magnetic dispersion of the undoped system and the doping dependence of the incommensurability they find good agreement with the inelastic neutron data for LBCO. The similarity between their constant-energy scans and those from spin-only approaches suggests that the damping due to the charge degrees of freedom does not play an essential rôle in the presence of charge and spin order. We presume that this is due to a partial freezing out of the charge degrees of freedom.

Aim of this Study and Set Up It is the aim of the present study to extend our previous investigations based on long-range stripe modulations in a single layer^{55,56} to bilayer cuprates such as YBCO. In addition, further results for single layers will be presented. All these results provide valuable guiding predictions for present and future inelastic neutron scattering experiments.

The article is set up as follows. In the next section, Sect. 2, the model will be introduced and its theoretical treatment will be explained. In Sect. 3 results for single layers will be presented. In the subsequent Sect. 4, results for two different modulation patterns in bilayers will be shown and compared. In Sect. 5 various scans at constant energy will be given. Finally, the conclusions will be drawn in Sect. 6.

2. Model and Calculation

Model In the Introduction we have motivated to consider the single-layer model sketched in Fig. 1. The Hamiltonian H is conveniently split into an intra-ladder part H_{ladder} and an inter-ladder part H_{inter}

$$H_{\text{ladder}} = \sum_{i \in \Gamma} J_{\perp} \mathbf{S}_i^L \cdot \mathbf{S}_i^R + J_{\parallel} (\mathbf{S}_i^L \cdot \mathbf{S}_{i+\delta_y}^L + \mathbf{S}_i^R \cdot \mathbf{S}_{i+\delta_y}^R) + J_{\text{cyc}} \sum_{i \in \Gamma} [(\mathbf{S}_i^L \cdot \mathbf{S}_i^R)(\mathbf{S}_{i+\delta_y}^L \cdot \mathbf{S}_{i+\delta_y}^R) + (\mathbf{S}_i^L \cdot \mathbf{S}_{i+\delta_y}^L)(\mathbf{S}_i^R \cdot \mathbf{S}_{i+\delta_y}^R) - (\mathbf{S}_i^L \cdot \mathbf{S}_{i+\delta_y}^R)(\mathbf{S}_{i+\delta_y}^L \cdot \mathbf{S}_i^R)] \quad (1)$$

where the superscripts L and R stand for the left and the right spin on a rung, respectively. The subscript $i = (i_x, i_y)$ denotes the rung by pointing to its center, i.e. the mid-point between the left (L) and the right (R) spin. The possible values are $\Gamma = a(4\mathbb{Z}, \mathbb{Z})$. The shift δ_y is given by $(0, a)$. The coupling between the spin ladders reads

$$H_{\text{inter}} = J' \sum_{i \in \Gamma} \mathbf{S}_i^R \cdot \mathbf{S}_{i+4\delta_x}^L, \quad (2)$$

where $\delta_x = (a, 0)$. As in the previous work we consider the isotropic spin ladder with $J := J_{\perp} = J_{\parallel}$ because the system is derived from a square lattice. The cyclic exchange (J_{cyc}) is known to be the dominant correction to the nearest-neighbour Heisenberg spin exchange.^{59–61} In the square lattice, its importance has been proposed⁶² and confirmed.^{63,64} Similarly, it has been proposed for two-leg spin ladders⁶⁵ and could be confirmed by the analysis of two-triplet bound states.^{66,67} We will use the thus established value $J_{\text{cyc}} = 0.2J_{\perp}$. Taking J_{cyc} into account is crucial if one aims at a quantitative agreement with experimental data.^{55,56} The effective exchange constant J' across the hole-rich stripes depends on the state of the eliminated charge degrees of freedom. The presence of holes substantially reduces J' relative to J .⁵⁵

In practice, we will fit J' to the experimental data; it takes a small ferromagnetic value ($J' < 0$) of a few percent of J .^{55,56}

Next we extend the above model from a single layer to a bilayer. We consider the two possibilities depicted in Fig. 2. There are, of course, still other patterns which can be considered. We focus on those in Fig. 2 due to their high symmetry.

Denoting the spins in the second layer by the superscripts R' and L' the coupling between the two layers reads

$$H_{\text{in-phase}} = J_s^{\text{ip}} \sum_{i \in \Gamma} (\mathbf{S}_i^L \cdot \mathbf{S}_i^{L'} + \mathbf{S}_i^R \cdot \mathbf{S}_i^{R'}) \quad (3)$$

$$H_{\text{out-of-phase}} = J_s^{\text{oop}} \sum_{i \in \Gamma} (\mathbf{S}_i^L \cdot \mathbf{S}_{i-2\delta_x}^{R'} + \mathbf{S}_i^R \cdot \mathbf{S}_{i+2\delta_x}^{L'}) \quad (4)$$

The exchange coupling J_s^{ip} takes small antiferromagnetic values ($J_s^{\text{ip}} > 0$). It corresponds to the interlayer exchange J_s determined for the undoped parent compound YBCO₆^{68,69} so that it should have about the same value. In case of YBCO₆, a value of $J_s \approx 0.08J$ has been deduced from the observation of optical magnons at around 70 meV^{68,69} and from a comparison of the two-magnon spectra in Raman scattering and in the optical conduc-

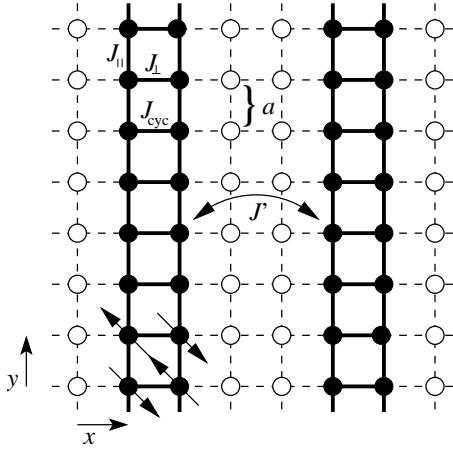


Fig. 1. Sketch of the model in a single cuprate plane. Each circle stands for a copper ion, i.e. the site of a spin 1/2 or a hole. The filled circles stand for the hole-poor regions where localized spins are assumed. The empty circles stand for the hole-rich stripes where itinerant behaviour is assumed. The spin-only model comprises only the localized spins which form a lattice of coupled two-leg ladders. The intraladder couplings are J_{\parallel} , J_{\perp} and J_{cyc} ; the interladder coupling J' is an effective coupling across the charged hole-rich stripes.

tivity.⁷⁰

In the coupling J_s^{oop} we do not denote the small superexchange processes to next-nearest neighbours. The coupling J_s^{oop} is an effective coupling which takes processes into account via the eliminated site (open circles in Fig. 2b). If there is a spin on the eliminated site there will be a ferromagnetic contribution to J_s^{oop} because both adjacent spins prefer to be antiparallel to it, hence parallel to each other. If the eliminated site is empty there will be an antiferromagnetic contribution to J_s^{oop} because the adjacent spins can undergo exchange processes. In total, the ferromagnetic and the antiferromagnetic contributions will partially cancel so that a small $|J_s^{\text{oop}}| < J_s^{\text{ip}}$ remains. Its sign is plausibly ferromagnetic since the eliminated site is occupied to 75% at doping 1/8. Note that the effective coupling J' between adjacent ladders was motivated in the same way.⁵⁵

Calculation: Single Layer The calculation runs in analogy to the one that we performed previously for the single layer.⁵⁵ A perturbative continuous unitary transformation (CUT) is performed for each ladder sep-

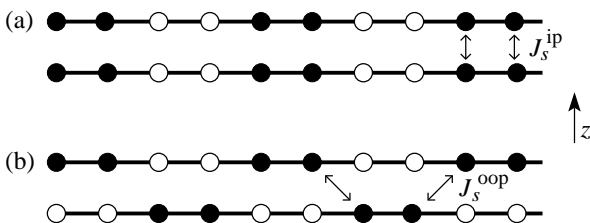


Fig. 2. Sideview of the two stripe-order patterns that we consider in bilayer systems (view along the y direction; open and full circles as in Fig. 1). The pattern in (a) assumes that the modulation is stacked; we will call this order in-phase. The pattern in (b) assumes that the modulation is alternating (out-of-phase).

arately.^{71, 72} Thereby, we obtain an effective model in terms of the elementary triplet excitations, triplons,⁷³ of the spin ladder. This effective model includes the one-triplon part $\sum_{k,\alpha} \omega_k^0 t_k^{\alpha,\dagger} t_k^\alpha$ where k is the wave vector along the ladder and $\alpha \in \{x, y, z\}$ is the flavour index for the three states of a triplon. The operator t_k^α stands for the annihilation of a triplon of flavour α with momentum k and $t_k^{\alpha,\dagger}$ stands for its creation. The dispersion ω_k^0 has been computed in many ways, see e.g. Refs.^{67, 71, 74–76} or Fig. 2a in Ref.⁵⁵

Besides the one-triplon part the effective model for the isolated ladder includes contributions involving two and more triplons. We neglect them since the one-triplon contribution dominates for the physically relevant parameters where 63% of the total spectral weight is in the one-triplon channel.⁵⁵

The coupling *between* the ladders can be written without a new comprehensive calculation. We apply the above unitary transformation U to each spin component at each site of a ladder yielding an effective observable

$$S_{i,\text{eff}}^{\alpha,\text{R}} := U^\dagger S_i^{\alpha,\text{R}} U = \sum_{m \in \mathbb{Z}} a_m (t_{i+m\delta_y}^{\alpha,\dagger} + t_{i+m\delta_y}^\alpha) + \dots \quad (5)$$

$$S_{i,\text{eff}}^{\alpha,\text{L}} = - \sum_{m \in \mathbb{Z}} a_m (t_{i+m\delta_y}^{\alpha,\dagger} + t_{i+m\delta_y}^\alpha) + \dots \quad (6)$$

Here t_i^α stands for the annihilation of a triplon of flavour α on the dimer i and $t_i^{\alpha,\dagger}$ stands for its creation. Consistent with the above approximation, the higher contributions involving two and more triplons are neglected.

First, we will use the identities (5) and (6) to find the transformed Hamiltonian for the interladder coupling. This can be done replacing the product of spin components $S_i^\alpha S_{i+4\delta_x}^\alpha$ by the right hand sides of Eqs. (5) and (6) taking into account that triplon operators on different ladders are involved. They are distinguished in real space by the x -component of i , i.e. i_x . In reciprocal space we use h for the momentum perpendicular to the ladders (k is the momentum along the ladders). This yields

$$H_{\text{inter}} = -J' \sum_{h,k;\alpha} d_{h,k} (t_{h,k}^{\alpha,\dagger} + t_{-h,-k}^\alpha) (t_{h,k}^\alpha + t_{-h,-k}^{\alpha,\dagger}) \quad (7)$$

where the minus sign results from the coupling of a right spin (on rung i) to a left spin (on $i+4\delta_x$). The momentum dependence is given by

$$d_{h,k} := \cos(8\pi h) a^2(k) \quad (8)$$

where h is measured in rlu; the cosine term captures the shift $4a$ from one ladder to the next one. The factor $a(k)$ is the Fourier transform of the coefficients a_m

$$a(k) = \sum_m \exp(i2\pi km) a_m. \quad (9)$$

The shape of the weight $a^2(k)$ has been illustrated in Fig. 2b in Ref.⁵⁵

The total Hamiltonian after the CUT and after the neglect of the multi-triplon parts is

$$H_{\text{ladder}} + H_{\text{inter}} = \quad (10)$$

$$\sum_{h,k;\alpha} \omega_k^0 t_k^{\alpha,\dagger} t_k^\alpha - J' d_{h,k} (t_{h,k}^{\alpha,\dagger} + t_{-h,-k}^\alpha) (t_{h,k}^\alpha + t_{-h,-k}^{\alpha,\dagger}).$$

It is bilinear in the triplon creation and annihilation operators so that it looks like a trivial one-particle problem. Unfortunately, this is not the case because the triplons are hard-core bosons. At maximum one of the three kinds may be present on a given rung. To make analytical progress, we exploit the fact that J' is small compared to the global energy scale J . Hence the off-diagonal terms such as $t_{-h,-k}^\alpha t_{h,k}^{\alpha,\dagger}$ and its hermitean conjugate are small and so will be the errors that are introduced by neglecting the hard-core constraint. If the hard-core constraint is neglected, that means the triplons are treated as ordinary bosons, the Hamiltonian (10) can be diagonalized by a standard Bogoliubov transformation. The resulting dispersion reads

$$\omega_{h,k} = \sqrt{(\omega_k^0)^2 - 4J'd_{h,k}\omega_k^0}. \quad (11)$$

Note that the omission of the hard-core constraint implies that there is only one mode per each momentum. The decay into two or more modes has been neglected. Thus we are dealing with a single-mode approximation.

At zero temperature, the dynamic structure factor $S_{h,k}(\omega)$ measures at which rate the system can be excited at a given momentum h, k and frequency ω . The excitation operator is the Fourier transform of the local spin components

$$S_{h,k}^\alpha = \frac{1}{\sqrt{N}} \sum_i e^{i2\pi(ki_x + hi_y)} \left(S_i^{\alpha,R} e^{i\pi h} + S_i^{\alpha,L} e^{-i\pi h} \right) \quad (12)$$

where we assume that the position of a rung is given by its center. Inserting Eqs. (5) and (6) leads to

$$S_{h,k}^\alpha = i \sin(\pi h) a(k) (t_{h,k}^{\alpha,\dagger} + t_{-h,-k}^\alpha). \quad (13)$$

The dynamic structure factor is the sum over all absolute excitation amplitudes squared, that means the square of the absolute values of the prefactors of the creation operators *after* the Bogoliubov diagonalization. The evaluation brings us to

$$S_{h,k}(\omega) = \sin^2(\pi h) a^2(k) \frac{\omega_k^0}{\omega_{h,k}} \delta(\omega - \omega_{h,k}). \quad (14)$$

If we add the contributions at negative frequencies proportional to $-\delta(\omega + \omega_{h,k})$ we may rewrite the expression as the imaginary part of a retarded response function

$$S_{h,k}(\omega) = -\frac{2}{\pi} \text{Im} \frac{\sin^2(\pi h) a^2(k) \omega_k^0}{(\omega + i0_+)^2 - \omega_{h,k}^2}. \quad (15)$$

The above formulae describe the single layer case.

Calculation: Bilayer Let us consider the in-phase pattern first. There is an obvious reflection symmetry between the two layers, cf. Fig. 2a. Hence the additional degree of freedom is accounted for most easily by distinguishing even ($\sigma = 1$) and odd triplons ($\sigma = -1$) with respect to the reflection. We will call this property the parity of the mode. The additional part of the Hamiltonian reads

$$H_{\text{in-phase}} = \quad (16)$$

$$J_s^{\text{ip}} \sum_{h,k,\sigma;\alpha} \sigma a^2(k) (t_{h,k,\sigma}^{\alpha,\dagger} + t_{-h,-k,\sigma}^\alpha) (t_{h,k,\sigma}^\alpha + t_{-h,-k,\sigma}^{\alpha,\dagger}).$$

We do not write down the remaining part of the Hamiltonian $H_{\text{ladder}} + H_{\text{inter}}$ because it is diagonal in σ ; it is given by Eq. 10 for each value of σ separately. The resulting dispersion depends on the parity σ ,

$$\omega_{h,k,\sigma}^{\text{ip}} = \sqrt{(\omega_k^0)^2 + 4a^2(k)\omega_k^0 (\sigma J_s^{\text{ip}} - J' \cos(8\pi h))}. \quad (17)$$

The corresponding dynamic structure factor depends on the parity σ only via the dispersion. So Eq. (15) is still applicable once $\omega_{h,k}$ is replaced by $\omega_{h,k,\sigma}^{\text{ip}}$.

Now we consider the out-of-phase pattern. There is no obvious reflection symmetry but a combination of reflection and translation symmetry. Let us assume that all the spin ladders lie in the same plane. Then the difference to the single layer calculation is the presence of the additional ladders located between those of a single layer. The exchange J' couples ladders at distance $4\delta_x$; the exchange J_s^{oop} couples spin ladders at distance $2\delta_x$. Then the whole problem has become a problem in a single plane. We can stick to the wave vector h which now is defined in a larger interval ($h \in [-1/4, 1/4]$ instead of $h \in [-1/8, 1/8]$) because also rungs with position i in $a(2\mathbb{Z}, \mathbb{Z})$ carry spins, not only those at $a(4\mathbb{Z}, \mathbb{Z})$. The additional contribution in the Hamiltonian is denoted

$$H_{\text{out-of-phase}} = -J_s^{\text{oop}} \sum_{h,k;\alpha} \cos(4\pi h) a^2(k) \cdot (t_{h,k}^{\alpha,\dagger} + t_{-h,-k}^\alpha) (t_{h,k}^\alpha + t_{-h,-k}^{\alpha,\dagger}). \quad (18)$$

where the cosine factor has half the argument of the cosine factor in Eq. (8) because the distance bridged is only half the one bridged by J' . The Bogoliubov diagonalization leads to the dispersion

$$\omega_{h,k} = \sqrt{(\omega_k^0)^2 - 4a^2(k)\omega_k^0 (J_s^{\text{oop}} \cos(4\pi h) + J' \cos(8\pi h))}. \quad (19)$$

Equations (18) and (19) start from the doubled Brillouin-zone interval for the transverse momentum h . In order to compare the in-phase and the out-of-phase patterns as closely as possible we prefer to stay with the Brillouin-zone interval of the in-phase pattern. The part of the branch of the out-of-phase pattern which is located at $|h| \in [1/8, 1/4]$ is folded back by the shift $h = h' \pm 1/4$. The backfolded branch can be identified with the *odd* one because the phase factor from a ladder in the lower layer to a ladder in the upper layer is $\exp(4\pi i h) = -\exp(4\pi i h')$, that means there is an extra factor -1 as it is characteristic for the odd mode. In the dispersion, we distinguish the two branches by $\sigma = \pm 1$

$$\omega_{h,k,\sigma}^{\text{oop}} = \sqrt{(\omega_k^0)^2 - 4a^2(k)\omega_k^0 (\sigma J_s^{\text{oop}} \cos(4\pi h) + J' \cos(8\pi h))}. \quad (20)$$

Note that we simplified the notation by passing from h' back to h . The corresponding dynamic structure factor is again the same as in the single layer calculation (15) except that $\omega_{h,k}$ is replaced by $\omega_{h,k,\sigma}^{\text{oop}}$. Note that the substitution $h \rightarrow h \pm 1/4$ does not apply to the sine-factor

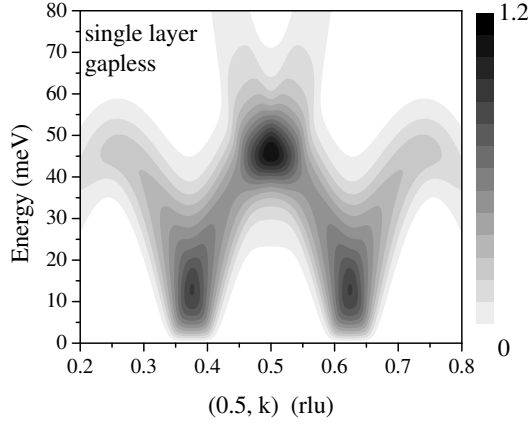


Fig. 3. Plot of the dynamic structure factor $\tilde{S}_{h,k}(\omega)$ in arbitrary units as function of momentum and energy. Note that $\tilde{S}_{h,k}(\omega)$ corresponds to the sum over regions with ladders running in x direction and regions with ladders running in y direction. The parameters apply to LBCO at doping $1/8$,^{5,55} namely $J = 127$ meV, $J_{\text{cyc}}/J = 0.2$ and $J' = -0.072J$. The energy resolution is 6 meV; it is implemented as the imaginary part η in $\omega \rightarrow \omega + i\eta$ in expression (15). The momentum resolution is $\Delta k = 0.03$ rlu which means that at a given momentum (h, k) the weight in the square $(h \pm \Delta k, k \pm \Delta k)$ is averaged. (Color online, gray scale in print version.)

in the structure factor (15). This is so because the matrix element to excite a local triplet depends only on the distance between the two spins on one rung. The phase factor between the layers does not matter.

Finally, we assume that regions with stripes running vertically and regions with stripes running horizontally are equally present in the samples. Hence we will display and discuss the symmetrized data $\tilde{S}_{h,k}(\omega) = (S_{h,k}(\omega) + S_{k,h}(\omega))/2$.

3. Single layer

Results for single layers are presented in our previous work.^{55,56} Very good agreement was obtained for realistic values of the coupling parameters. In particular, it was shown that significant cyclic exchange ($J_{\text{cyc}}/J \approx 0.2$) is needed to reconcile the resonance energy and the global energy scale. In the framework of the stripe model the resonance appears as the saddle point in a strongly anisotropic dispersion.^{54,55} The dispersion is very large along the ladders, i.e. along the stripes, while it is small perpendicular to them. The global energy scale is set by the maximum of the dispersion. It can be determined from the analysis of the dispersion itself⁵⁶ or from the analysis of the momentum-integrated structure factor.⁵⁵

For LBCO at $1/8$ doping, the global energy scale is $J = 127$ meV and the interladder coupling is $J' = -0.072J$. This value corresponds to the quantum critical point where the spin-liquid gap just vanishes. The actual value will be a little larger because there is evidence for (weak) long-range magnetic order.²⁸

Using the single-layer model, the analysis for underdoped YBCO_{6.6} yields $J = 114$ meV and the interladder coupling $J' = -0.035J$.⁵⁶ The significantly smaller value of J' is implied by the presence of a finite spin gap.

A cut through the Brillouin zone is displayed in Fig. 3.

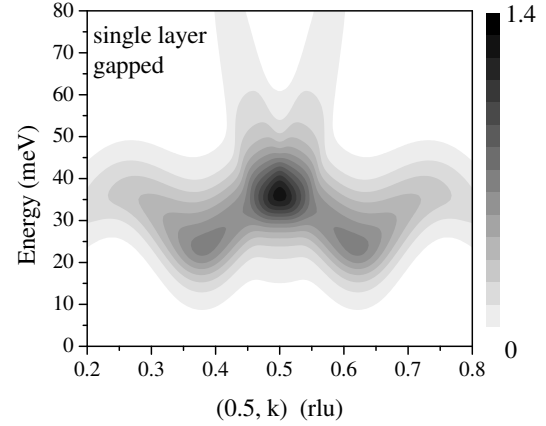


Fig. 4. Plot of the dynamic structure factor $\tilde{S}_{h,k}(\omega)$ in arbitrary units as function of momentum and energy. Based on the single-layer model, the parameters apply to underdoped YBCO_{6.6},^{4,56} namely $J = 114$ meV, $J_{\text{cyc}}/J = 0.2$ and $J' = -0.035J$. The plot is to be compared with Fig. 1i in Ref.⁴ The resolutions are chosen as for Fig. 3. (Color online, gray scale in print version.)

The cut runs parallel to the reciprocal axis through the antiferromagnetic wave vector $\mathbf{Q}_{\text{AF}} = (1/2, 1/2)$. Both the energy dependence and the momentum dependence can be discerned. The values chosen are those which apply to LBCO; finite resolutions in energy and in momentum are taken into account.

Around 45 meV a patch of high intensity at \mathbf{Q}_{AF} is clearly visible. To lower energy the intensity decreases rapidly, becoming significant again at low energies of 10-20 meV. There is finite intensity down to the lowest energies since the system is gapless. It is very remarkable that the finite resolutions lead to the impression of almost vertical rods of high intensity (dark (online: yellow) patches) at the incommensurate positions $(1/2, 1/2 \pm 1/8)$. This coincides nicely with the observations of many experiments, see e.g. the generic graph discussed in Fig. 13b in Ref.¹ We emphasize that the underlying dispersion is sine-shaped as expected, see e.g. Fig. 1 in Ref.⁵⁶

In Fig. 4 the corresponding graph is shown for a gapped system with parameters which apply to underdoped YBCO_{6.6} (Ref.⁴) on the basis of the single-layer model. The theoretical result agrees well with Fig. 1i in Ref.⁴. Clearly, the resonance is dominating and there are tails of intensity to lower energy which point to incommensurate momenta. The intensity toward lower energies is quickly decreasing both in theory and experiment. Discrepancies are seen in the width of the resonance patch which is larger in experiment. It appears also that the shift away from \mathbf{Q}_{AF} is experimentally lower than in our calculation. Since the experimental result is obtained via the subtraction of a background it cannot be excluded that finer features are lost in experiment. Measurements with improved resolution and signal strength will be very interesting to elucidate further details.

4. Bilayer

Now we turn to the properties of bilayer compounds such as YBCO. Before we present results some considerations on the two patterns under study are in order. It

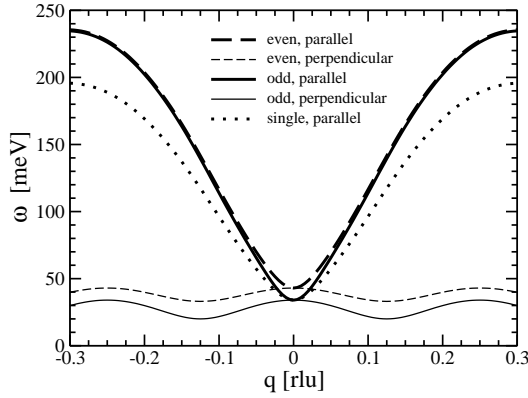


Fig. 5. Dispersion of the odd (solid) and the even (dashed) mode for the in-phase pattern as function of q , the distance to the antiferromagnetic wave vector \mathbf{Q}_{AF} . The thin lines show the dispersion perpendicular to the spin ladders; the thick lines show the dispersion parallel to the spin ladders. The parameters are $J = 136$ meV, $J_s^{\text{ip}} = 0.022J$, $J' = -0.024J$ and $J_{\text{cyc}} = 0.2J$, corresponding to $\Delta = 20$ meV, $\omega_{\text{res}}^{\text{even}} = 43$ meV and $\omega_{\text{res}}^{\text{odd}} = 34$ meV. The dotted line depicts the dispersion in a single layer with $J = 114$ meV, $J' = -0.035J$ and $J_{\text{cyc}} = 0.2J$, corresponding to $\Delta = 20$ meV and $\omega_{\text{res}} = 34$ meV. For these parameters, the dispersion perpendicular to the ladders in the single-layer model (not shown) is indistinguishable from the dispersion of the odd bilayer mode (thin solid line).

is plausible that the out-of-phase pattern is energetically favoured because the charges (the holes in the stripes) are more evenly distributed, see Fig. 2. An even distribution lowers the long-range Coulomb potential. Evidence for such interlayer correlations has been reported on the basis of a hard x-ray diffraction study of Nd-doped LSCO.¹² There, stripes in next-nearest-neighbour layers are found in an out-of-phase arrangement. Note that in this particular case, the nearest-neighbour layers are probably decoupled because the stripes on adjacent layers are running in orthogonal directions due to the coupling to the lattice via the tilting of the oxygen octahedra.

The models for the bilayer have one additional parameter, namely the interlayer coupling. The approximate size of this coupling was discussed above following Eq. (4). We have determined the set of coupling parameters in the following way. We fix the cyclic exchange at the established value of $J_{\text{cyc}}/J = 0.2$ (see above and Refs.^{63,64,67}). The remaining three parameters J , J' and $J_s^{\text{ip/op}}$ are determined from the experimental values for the spin gap ($\Delta = 20$ meV in YBCO_{6.6}, Ref.⁷⁷) and for the energy of the resonance mode in the odd ($\omega_{\text{res}}^{\text{odd}}$) and in the even channel ($\omega_{\text{res}}^{\text{even}}$). In both channels, the resonance mode corresponds to a saddle point in the two-dimensional, anisotropic dispersion. In underdoped YBCO_{6.6} the odd resonance lies at about $\omega_{\text{res}}^{\text{odd}} = 34$ meV.⁴ Unfortunately, the even resonance has not yet been observed at this doping level. In a slightly overdoped sample, the resonances have been observed at $\omega_{\text{res}}^{\text{even}} = 43$ meV and $\omega_{\text{res}}^{\text{odd}} = 36$ meV.⁷⁸ Since the value of the odd resonance is very similar to the result for YBCO_{6.6}, we assume that also the even resonance is similar and choose $\omega_{\text{res}}^{\text{even}} = 43$ meV and $\omega_{\text{res}}^{\text{odd}} = 34$ meV.

The resulting set of coupling parameters reads $J =$

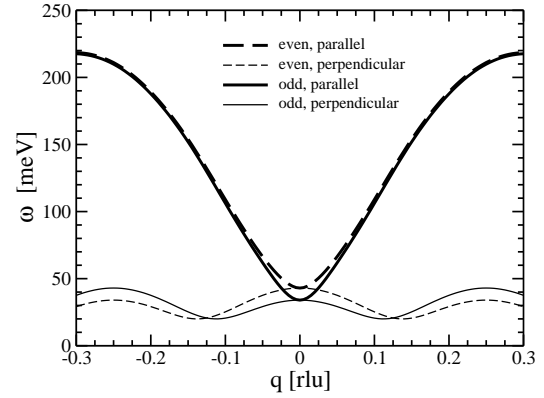


Fig. 6. Dispersion of the odd (solid) and the even (dashed) mode for the out-of-phase pattern as function of q as in Fig. 5. The parameters are $J = 126$ meV, $J_s^{\text{op}} = -0.026J$, $J' = -0.040J$ and $J_{\text{cyc}} = 0.2J$.

136 meV, $J_s^{\text{ip}} = 0.022J$ and $J' = -0.024J$ for the in-phase pattern and $J = 126$ meV, $J_s^{\text{op}} = -0.026J$ and $J' = -0.040J$ for the out-of-phase pattern. These two sets will be used in all the plots shown in the following. First, we note that J_s^{ip} is indeed antiferromagnetic and J_s^{op} is ferromagnetic. Second, the absolute value of J_s^{ip} is fairly small, much smaller than the interlayer coupling in undoped YBCO₆ of $0.08J$. This is another indication that the out-of-phase pattern is more realistic.

Note that J and J' do not change much in the bilayer analyses with respect to the single layer model. The parameter sets all are in an experimentally reasonable range.

In Fig. 5 the dispersions for a single layer and for the bilayer with in-phase pattern are shown. The low-lying dispersion perpendicular to the spin ladders is (almost) the same for the odd mode and for the single layer. This fact corroborates the often made statement that the physics of the odd mode in the bilayer is well described in a model of a single layer. But this does not hold for the dispersion parallel to the spin ladders where the single-layer model implies a significantly lower maximum value. This results from the larger energy scale $J = 136$ meV (instead of 114 meV) needed to meet the resonance energies and the spin gap. The calculated dispersion of the odd mode appears to be steeper than observed experimentally,⁴ but this will have to be clarified by more detailed experiments.

It is striking that the odd and the even mode energies are almost identical above the resonance energies, i.e. above ≈ 50 meV. This can be attributed to the weight factor $a^2(k)$ in Eq. 17, which suppresses the difference between the even and the odd mode for small momenta k (see Fig. 2b in Ref.⁵⁵). At low energies, i.e., $k \approx 0.5$ rlu parallel to the ladders, the coupling between the layers leads to the expected splitting of the two modes.

In Fig. 6, the dispersions for the bilayer with out-of-phase pattern are shown. Again, the odd and the even dispersion almost coincide at energies above the resonances (saddle points). The total dispersion is lower than the one for the in-phase pattern in Fig. 5 but still higher than in the single-layer model.

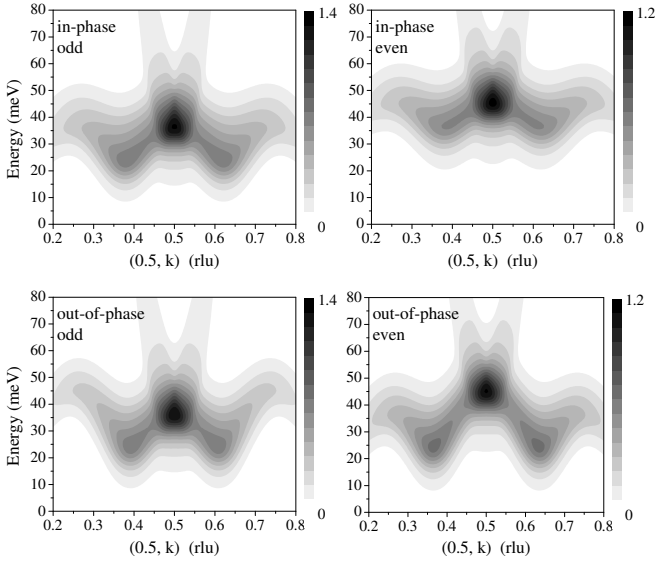


Fig. 7. Plots of the dynamic structure factor $\tilde{S}_{h,k}(\omega)$ (15) for the coupling values as in Figs. 5 and 6. The resolutions in energy and momentum are those used also in Fig. 3. (Color online, gray scale in print version.)

At low energies, the behaviour of the dispersion perpendicular to the ladders is remarkable. It is not just a splitting but the dispersion of one mode can be obtained from the dispersion of the other mode by a translation by $1/4$ rlu perpendicular to the ladders. This is obvious in view of the derivation of the dispersions from the common expression (19). If the dispersion of the even mode can be detected, our predictions in Figs. 5 and 6 will allow to distinguish both correlation patterns clearly. The observation of a splitting at $(1/2, 1/2 \pm 1/8)$ would support the in-phase pattern; the absence of such a splitting would corroborate the out-of-phase scenario. Note that in the out-of-phase pattern *both* modes have the same minimum energy, i.e. the same spin gap.

Another very noteworthy observation concerns the position where the minimum energy is reached. In spite of the underlying commensurate charge modulation, the spin gap is not reached at $q = \pm 1/8$ but at a smaller value (in the odd channel). This results from the sum of the two cosine-terms under the square root in the dispersion (20). Clearly, this effect will be enhanced if J_s^{op} increases relative to J' . It opens up the possibility to vary the incommensurability continuously *without* any change in the periodicity of the charge modulation. This may give rise to a difference in the saturation value of the incommensurability between single layer and bilayer compounds. Such a difference has been discussed in the literature (LSCO:⁹ $\approx 1/8$; YBCO:⁷⁹ $\approx 1/10$). Note, however, that the determination of the incommensurability may be hampered by the asymmetric distribution of the spectral weight (see below).

The Figs. 5 and 6 do not provide information on the intensities. This experimentally crucial information is displayed in Fig. 7. The resonance at \mathbf{Q}_{AF} is dominating in all four plots. The intensity decreases significantly towards lower energies. The response of the odd modes is

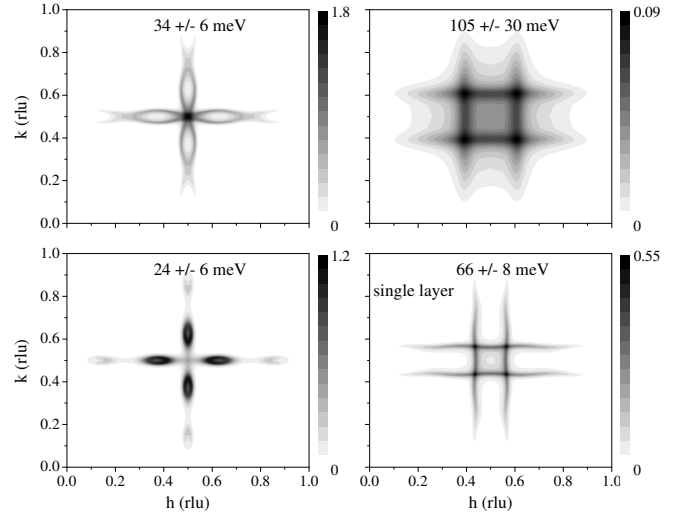


Fig. 8. Constant-energy scans for the single-layer model. The energies and the energy resolutions are given in the figure. There is no broadening in momentum space which must be kept in mind when comparing to experimental data.⁴ The couplings are $J = 114$ meV, $J_{\text{cyc}}/J = 0.2$ and $J' = -0.035J$.⁵⁶ (Color online, gray scale in print version.)

fairly similar to the response in a single layer (see Fig. 4), in particular the response for the in-phase pattern. For the out-of-phase pattern, the odd response displays the interesting feature that the resonance is lower in energy than the local maxima of the dispersion at $k = 1/2 \pm 1/4$.

By construction, the resonance of the even modes lies higher in energy. For the in-phase pattern the whole response is located at higher energies than in the odd channel. For the out-of-phase pattern this is not true. There, the intensity of the even mode reaches down to the spin-gap energy of the odd channel. Opposite to the behaviour of the odd dispersion, the local maxima at $k = 1/2 \pm 1/4$ in the even channel are located at lower energies than the even resonance itself.

The results for the odd mode are certainly consistent with the available experimental data. Our spin-only model, however, predicts almost the same intensities for the even and the odd modes. This is at odds with experiment where it seems to be extremely difficult to detect the even mode at all. We presume that the energetically higher lying even modes are affected more strongly by damping effects, for instance due to the eliminated charge degrees of freedom and due to the hard-core triplon-triplon interaction. A strong damping may hinder the experimental observability significantly. This issue certainly calls for further theoretical investigations. However, the damping should be less important at low energies. Thus detailed experimental investigations of the spin gap in the even channel appear very promising.

5. Constant-Energy Scans

The observations made in the previous section are supported by constant-energy scans. For comparison we include in Fig. 8 four scans for a single layer. The energies and the energy resolutions chosen correspond to the experimental ones.⁴ The scan at 24 meV is very close

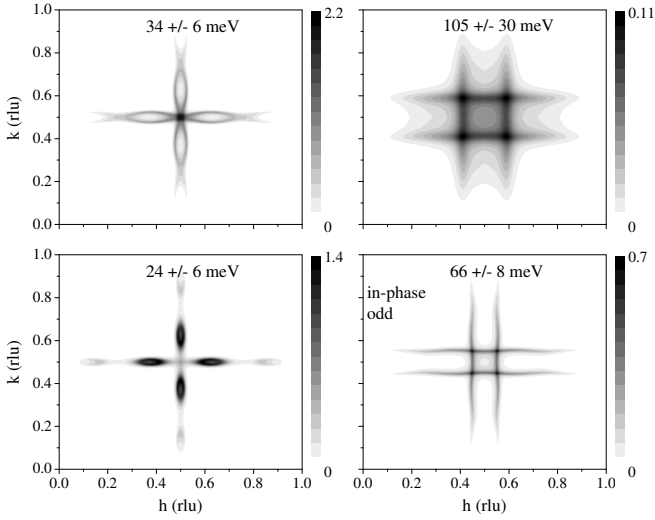


Fig. 9. Constant-energy scans for the odd mode in the in-phase bilayer model. The parameters are $J = 136$ meV, $J_s^{\text{ip}} = 0.022J$, $J' = -0.024J$ and $J_{\text{cyc}} = 0.2J$. (Color online, gray scale in print version.)

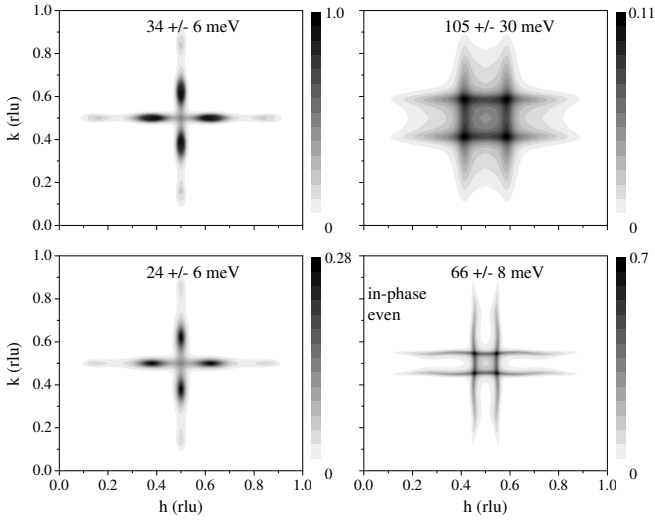


Fig. 10. Constant-energy scans for the even mode in the in-phase bilayer model. Parameters are the same as for Fig. 9. (Color online, gray scale in print version.)

to the spin gap, i.e. the lower bound of the magnetic excitations. The scan at 34 meV provides data at the resonance energy which corresponds to the saddle point of the dispersion.^{55,56} The two remaining scans provide information at energies above the saddle point.

The theoretical results agree very well with the experimental findings.⁴ In particular, one has a diamond-like shape at low energies of four incommensurate satellites which merge at the resonance energy to an almost circular single patch at \mathbf{Q}_{AF} . Note that already at 24 meV the peak intensity has shifted towards \mathbf{Q}_{AF} , which may blur the precise value of the incommensurability in the analysis of experimental data. Above the resonance energy the shape is square-like with maxima of the intensity at the corners. The theoretical result at higher energies displays a very low intensity at \mathbf{Q}_{AF} while the experiment

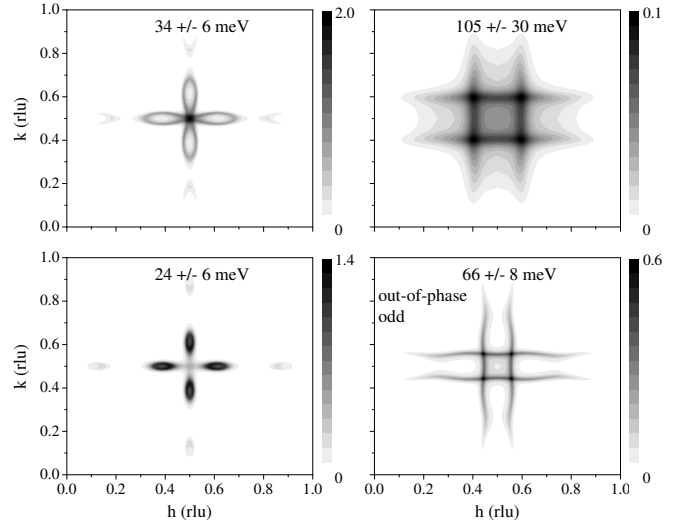


Fig. 11. Constant-energy scans for the odd mode in the out-of-phase bilayer model. The parameters are $J = 126$ meV, $J_s^{\text{oop}} = -0.026J$, $J' = -0.040J$ and $J_{\text{cyc}} = 0.2J$. (Color online, gray scale in print version.)

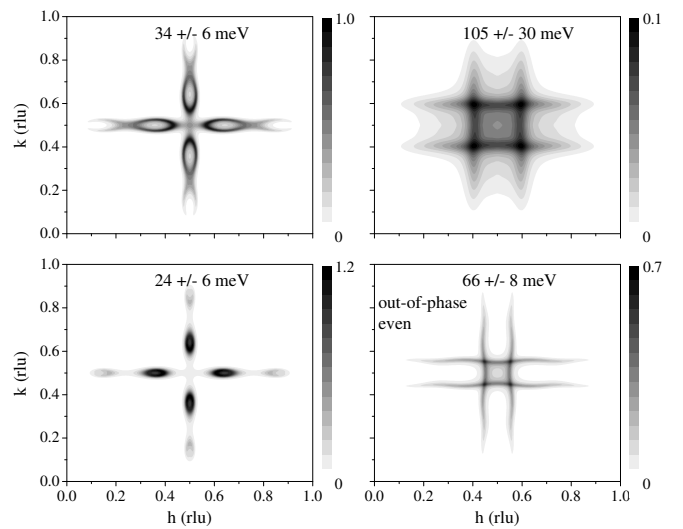


Fig. 12. Constant-energy scans for the even mode in the out-of-phase bilayer model. Parameters are the same as for Fig. 11. (Color online, gray scale in print version.)

shows squares with non-negligible intensity inside. Furthermore, the tails of intensity outside the squares are only very vaguely seen in experiment. We attribute both features to multi-triplon contributions and life-time effects⁵⁵ which we neglected in our approach. But in view of the simplicity of the model, the agreement obtained is remarkable.

In Fig. 9 the same scans are depicted for the odd triplon in the in-phase pattern. Qualitatively, these plots are identical to the ones for the single layer in Fig. 8. At low energies this is even true on a quantitative level which can be taken as an argument that a single-layer calculation captures a significant portion of the physics of the odd modes in a bilayer system. At higher energies, however, the structures are narrower (i.e. closer to \mathbf{Q}_{AF})

in the bilayer due to the larger value of J , as mentioned in the discussion of the dispersion shown in Fig. 5.

In Fig. 10 the scans for the even mode are shown. At high energies they are almost identical to those for the odd mode in Fig. 9. The most striking differences occur at low energies where the intensities are much lower. Note that the scan at 24 meV runs *below* the spin gap of the even mode, the finite intensity is caused only by the broadening. The scans for the odd and the even mode at 34 meV differ decisively because only in the former case the saddle point is hit. This explains the differences in shape and in maximum intensity.

The results for the out-of-phase pattern are presented in Figs. 11 and 12. Again, the odd and the even response are almost identical at high energies while they differ at lower energies. The most striking difference is whether the resonant saddle point is hit (at 34 meV for the odd mode) or not (at 34 meV for the even mode). Very interesting is the situation at 24 meV. In the in-phase pattern (see Figs. 9 and 10) the even mode and the odd mode yield the same shape but the intensity differs by a factor of 5. In the out-of-phase pattern there is no significant difference in the intensities between the odd and the even result. But a closer look reveals that the diamond in the odd channel is smaller than the one in the even channel (see also the dispersion in Fig. 6). This results from the fact that in spite of the given charge modulation the position of the minima depends on the ratio of the prefactors of the two cosine-terms in the dispersion (20), in particular on the sign of this ratio. For ferromagnetic $J_s^{\text{oop}} < 0$ the minima in the odd channel are closer to \mathbf{Q}_{AF} than without interlayer coupling while the minima in the even channel are further away from \mathbf{Q}_{AF} . These low energy features should be robust against the damping by charge degrees of freedom and thus appear as promising candidates for future experiments.

6. Conclusions

We investigated a spin-only model with stripe order in a single layer and for two patterns in a bilayer. In the first pattern, the stripes and hence the spin ladders are *in-phase* in the two layers; in the second pattern they are arranged *out-of-phase*, see Fig. 2. The patterns are taken to be long-range in our calculation. But for systems like YBCO we view the assumption of long-range stripe order as an approximation to fluctuating medium-range correlations. This approximation significantly eases the theoretical treatment.

The calculation was done by coupling the effective model, which was obtained previously for isolated spin ladders with cyclic exchange by continuous unitary transformations. The effective model is formulated in terms of triplons, the elementary triplet excitations. The coupling *between* the ladders is small so that the neglect of the hard-core constraint of the triplons is justified. Thereby, we can obtain quantitative results.

The results obtained within the single-layer model agree very well with experimental findings, both for gapless^{5,55} and for gapped systems.^{4,56} We stress that the coupling parameters J and J_{cyc} are realistic ones and that only one parameter (J') has not been derived inde-

pendently from other experiments. In the gapless case we have shown that the finite resolution in momentum and energy leads to the impression of almost vertical rods in the (ω, k) plane (Fig. 3), very much like what is seen in many experiments. In the gapped phase, our calculation reproduces the experimentally observed rapid decrease of intensity towards lower energies.

In the bilayer system we distinguish contributions from the odd and from the even triplon mode. Independent of the stripe pattern considered the result in the odd channel resembles very much what is obtained for a single layer. This finding confirms the often used assumption that a model with a single layer suffices to capture the physics in the odd channel of the bilayer system. The agreement between odd channel and single-layer results is almost quantitative for the in-phase stripe correlations, at least at low energies. For the out-of-phase pattern, the odd mode dispersion does not have its minimum at $(1/2, 1/2 \pm \delta)$ with $\delta = 1/8$, but at smaller values $\delta < 1/8$. So we have discovered a way to reconcile values of δ different from $1/8$ with a charge correlation dominated by the periodicity $4a$.

The even modes behave almost quantitatively like the odd modes at energies higher than the resonance energies. At energies of the order of the resonance energies the even and odd modes split. In the in-phase pattern this splitting does not depend on the momentum h perpendicular to the ladders. In the out-of-phase pattern, however, the even mode dispersion and the odd mode dispersion can be derived from each other by a translation by $1/4$ rlu perpendicular to the stripes. This implies that both modes have the same spin gap, that means the intensity of the even modes reaches also down to low energies. Furthermore, we predict that the even mode displays a larger shift in the position of its minima located at $(1/2, 1/2 \pm \delta)$ with $\delta > 1/8$. These predictions can be tested experimentally if the even mode can be observed.

One serious discrepancy between theory and experiment arises from the relative intensities of the even and the odd modes. The even mode is hardly seen in experiment. So far it is only seen in the undoped parent compound YBCO₆^{68,69} and in a slightly overdoped, Ca substituted sample Y_{0.9}Ca_{0.1}Ba₂Cu₃O₇.⁷⁸ In the latter sample the intensity is reduced by a factor of 3 with respect to the odd mode whereas our calculation implies that the reduction in intensity should only be about 20%. This discrepancy can possibly be attributed to the stronger damping that the even mode experiences because it lies at higher energy. A significant damping broadens the response so that it becomes difficult to distinguish from the omnipresent backgrounds, thus the signal is lost. The damping might be due to (i) the eliminated charge degrees of freedom, (ii) the hard-core interaction between the triplons or (iii) multi-triplon contributions. The issue which processes are the important ones must be left to future research.

In this context one may also speculate about a possible doping dependence of $\omega_{\text{res}}^{\text{even}}$. Experimentally, it has been established that the *odd* resonance shifts to lower energies with decreasing doping.³ Assuming that this shift

is at least partly caused by an increase of the modulus of the interlayer coupling $J_s^{\text{ip/ooP}}$, it corresponds to an increase of $\omega_{\text{res}}^{\text{even}}$ with decreasing doping, and thus also to an increased damping of the even mode.

We advocate the out-of-phase pattern as the more likely candidate to describe the relevant bilayer correlations. First, the concomitant charge distribution is more even, so the Coulomb interaction favours the out-of-phase pattern. Second, the small value of the interlayer coupling of about 2-3% of J (compared to 8% in the undoped parent compound) is indicative that it is not the direct exchange from one layer to the other as in Fig. 2a which is responsible for the interlayer coupling. For the out-of-phase pattern shown in Fig. 2b it is natural to assume that the (absolute) value of J_s^{op} is small. Third, it is appealing to attribute values of the incommensurability different from $1/8$ to the tunable incommensurability in the out-of-phase pattern.

It is remarkable to which extent the straightforward model of coupled spin ladders describes the emerging universal behaviour of the magnetic excitations in high-temperature superconducting cuprates. This is even more fascinating in view of the fact that static stripes are not supported by experiment³⁷ and of the tendency to form more two-dimensional tiling patterns, at least at the surfaces.^{44,80} We think that the universal behaviour of the magnetic excitations may be explained by assuming that on a medium-range of 4 to 8 lattice spacings the correlations are similar to those of stripes. It is plausible that our results for not too low energies remain qualitatively valid for such a system with medium-range stripe correlations. Definitely, more work is called for to improve the theoretical description further.

Equally, further high-resolution neutron experiments are desirable in order to test the predictions made in the present work. This will provide deeper insight in the complex physics of the elementary excitations of the cuprate superconductors.

Acknowledgment

Helpful discussions are acknowledged with M. Braden, B. Keimer, S. Sachdev, J.M. Tranquada, M. Vojta and T. Yokoo. This work was supported by the DFG in SFB 608 and in SP 1073 as well as by the COE at the Tohoku University, Sendai, where a part of this work was done during a visiting professorship of one of us (GSU).

- 1) H. B. Brom and J. Zaanen, in *Handbook of Magnetic Materials*, by K. H. J. Buschow, vol. 15, p. 379 (Elsevier, New York, 2003)
- 2) M. R. Norman and C. Pépin, Rep. Prog. Phys. **66** (2003) 1547.
- 3) Y. Sidis, S. Pailhès, B. Keimer, P. Bourges, C. Ulrich and L. P. Renault, phys. stat. sol. **241** (2004) 1204.
- 4) S. M. Hayden, H. A. Mook, P. Dai, T. G. Perring and F. Doğan, Nature **429** (2004) 531.
- 5) J. M. Tranquada, H. Woo, T. G. Perring, H. Goka, G. D. Gu, G. Xu, M. Fujita and K. Yamada, Nature **429** (2004) 534.
- 6) N. B. Christensen, D. F. McMorrow, H. M. Ronnow, B. Lake, S. M. Hayden, G. Aeppli, T. G. Perring, M. Mangkorntong, M. Nohara and H. Tagaki, cond-mat/0403439.
- 7) S. Wakimoto, G. Shirane, Y. Endoh, K. Hirota, S. Ueki, K. Yamada, R. J. Birgeneau, M. A. Kastner, Y. S. Lee, P. M. Gehring

- and S. H. Lee, Phys. Rev. B **60** (1999) R769.
- 8) M. Fujita, K. Yamada, H. Hiraka, P. M. Gehring, S. H. Lee, S. Wakimoto and G. Shirane, Phys. Rev. B **65** (2002) 064505.
- 9) K. Yamada, C. H. Lee, K. Kurahashi, J. Wada, S. Wakimoto, S. Ueki, H. Kimura, Y. Endoh, S. Hosoya, G. Shirane, R. J. Birgeneau, M. Greven, M. A. Kastner and Y. J. Kim, Phys. Rev. B **57** (1998) 6165.
- 10) A. H. Castro Neto and C. Morais Smith, cond-mat/0304094.
- 11) J. M. Tranquada, B. J. Sternlieb, J. D. Axe, Y. Nakamura and S. Uchida, Nature **375** (1995) 561.
- 12) M. v. Zimmermann, A. Vigliante, T. Niemöller, N. Ichikawa, T. Frello, J. Madsen, P. Wochner, S. Uchida, N. H. Andersen, J. M. Tranquada, D. Gibbs and J. R. Schneider, Europhys. Lett. **41** (1998) 629.
- 13) S.-W. Cheong, G. Aeppli, T. E. Mason, H. Mook, S. M. Hayden, P. C. Canfield, Z. Fisk, K. N. Clausen and J. L. Martinez, Phys. Rev. Lett. **67** (1991) 1791.
- 14) T. E. Mason, A. Schröder, G. Aeppli, H. A. Mook and S. M. Hayden, Phys. Rev. Lett. **77** (1996) 1604.
- 15) G. Aeppli, S. M. Hayden, P. Dai, H. A. Mook, R. D. Hung, T. G. Perring and F. Dogan, Science **278** (1997) 1432.
- 16) B. Lake, G. Aeppli, T. E. Mason, A. Schröder, D. F. McMorrow, K. Lefmann, M. Isshiki, M. Nohara, H. Takagi and S. M. Hayden, Nature **400** (1999) 43.
- 17) H. Hiraka, Y. Endoh, M. Fujita, Y. S. Lee, J. Kulda, A. Ivanov and R. J. Birgeneau, J. Phys. Soc. Jpn. **70** (2001) 853.
- 18) J. M. Tranquada, C. H. Lee, K. Yamada, Y. S. Lee, L. P. Regnault and H. M. Ronnow, Phys. Rev. B **69** (2004) 174507.
- 19) J. Rossat-Mignot, L. P. Regnault, C. Vettier, P. Bourges, P. Burlet, J. Bossy, J. Y. Henry and G. Lapertot, Physica **C185-189** (1991) 86.
- 20) H. He, P. Bourges, Y. Sidis, C. Ulrich, L. P. Regnault, S. Pailhès, N. S. Berzigiarova, N. N. Kolesnikov and B. Keimer, Science **295** (2002) 1045.
- 21) M. Arai, T. Nishijima, Y. Endoh, T. Egami, S. Tajima, K. Tomimoto, Y. Shiohara, M. Takahashi, A. Garrett and S. M. Bennington, Phys. Rev. Lett. **83** (1999) 608.
- 22) P. Bourges, Y. Sidis, H. F. Fong, L. P. Regnault, J. Bossy, A. Ivanov and B. Keimer, Science **288** (2000) 1234.
- 23) D. Reznik, P. Bourges, L. Pintschovius, Y. Endoh, Y. Sidis, Y. Shiokara and S. Tajima, Phys. Rev. Lett. **93** (2004) 207003.
- 24) T. Yokoo, M. Arai, Y. Shiohara, S. Tajima, C. D. Frost and Y. Endoh, Physica **C388** (2003) 223.
- 25) T. Yokoo, M. Arai, Y. Shiohara, S. Tajima, C. D. Frost and Y. Endoh, J. Low Temp. Phys. **131** (2003) 731.
- 26) H. A. Mook, P. C. Dai and F. Dogan, Phys. Rev. Lett. **88** (2002) 097004.
- 27) A. R. Moodenbaugh, Y. Xu, M. Suenaga, T. J. Folkerts and R. N. Shelton, Phys. Rev. B **38** (1988) 4596.
- 28) M. Fujita, H. Goka, K. Yamada, J. M. Tranquada and L. P. Regnault, Phys. Rev. B **70** (2004) 104517.
- 29) D. K. Morr and D. Pines, Phys. Rev. Lett. **81** (1998) 1086.
- 30) A. Abanov and A. V. Chubukov, Phys. Rev. Lett. **83** (1999) 1652.
- 31) H. J. Schulz, J. Phys. I France **50** (1989) 2833.
- 32) J. Zaanen and O. Gunnarsson, Phys. Rev. B **40** (1989) 7391.
- 33) C. H. Chen, S.-W. Cheong and A. S. Cooper, Phys. Rev. Lett. **71** (1993) 2461.
- 34) J. M. Tranquada, D. J. Buttrey, V. Sachan and J. E. Lorenzo, Phys. Rev. Lett. **73** (1994) 1003.
- 35) H.-H. Klauss, W. Wagener, M. Hillberg, W. Koopmann, H. Walf, F. J. Litterst, M. Hücker and B. Büchner, Phys. Rev. Lett. **85** (2000) 4590.
- 36) L. Balents, L. Bartosch, A. Burkov, S. Sachdev and K. Sengupta, cond-mat/0409470.
- 37) V. Hinkov, S. Pailhès, P. Bourges, Y. Sidis, A. Ivanov, A. Kulakov, C.T. Lin, D.P. Chen, C. Bernhard and B. Keimer, Nature **430** (2004) 650.
- 38) V. J. Emery, S. A. Kivelson and O. Zachar, Phys. Rev. B **56** (1997) 6120.
- 39) S. A. Kivelson, I. P. Bindloss, E. Fradkin, V. Oganessian, J. M. Tranquada, A. Kapitulnik and C. Howald, Rev. Mod. Phys. **75** (2003) 1201.

- 40) V. I. Anisimov, M.A. Korotin, A.S. Mylnikova, A.V. Kozhevnikov and J. Lorenzana, *cond-mat/0402162*.
- 41) H. J. Schulz, *Phys. Rev. B* **34** (1986) 6372.
- 42) E. Dagotto and T. M. Rice, *Science* **271** (1996) 618.
- 43) J. Tworzydło, O. Y. Osman, C. N. A. van Duin and J. Zaanen, *Phys. Rev. B* **59** (1999) 115.
- 44) T. Hanaguri, C. Lupien, Y. Kohsaka, D.-H. Lee, M. Azuma, M. Takano, H. Takagi and J. C. Davis, *Nature* **430** (2004) 1001.
- 45) A. P. Schnyder, A. Bill, C. Mudry, R. Gilardi, H. M. Rønnow and J. Mesot, *Phys. Rev. B* **70** (2004) 214511.
- 46) D. Zanchi and H. J. Schulz, *Phys. Rev. B* **61** (2000) 13609.
- 47) N. Furukawa, C. Honerkamp, M. Salmhofer and T. M. Rice, *Physica B* **284** (2000) 1575.
- 48) C. J. Halboth and W. Metzner, *Phys. Rev. B* **61** (2000) 7364.
- 49) A. Abanov, A. V. Chubukov and J. Schmalian, *Adv. Phys.* **52** (2003) 119.
- 50) S. Schmitt-Rink, C. M. Varma and A. E. Ruckenstein, *Phys. Rev. Lett.* **60** (1988) 2793.
- 51) E. Dagotto, *Rev. Mod. Phys.* **66** (1994) 763.
- 52) E. Demler, W. Hanke and S.-C. Zhang, *Rev. Mod. Phys.* **76** (2004) 909.
- 53) L. Balents, L. Bartosch, A. Burkov, S. Sachdev and K. Sengupta, *cond-mat/0408329*.
- 54) M. Vojta and T. Ulbricht, *Phys. Rev. Lett.* **93** (2004) 127002.
- 55) G. S. Uhrig, K. P. Schmidt and M. Grüninger, *Phys. Rev. Lett.* **93** (2004) 267003.
- 56) G. S. Uhrig, K. P. Schmidt and M. Grüninger, *J. Mag. Mag. Mat. in press* (2005)
- 57) M. Vojta and S. Sachdev, *cond-mat/0408461*.
- 58) G. Seibold and J. Lorenzana, *cond-mat/0406589*.
- 59) H. J. Schmidt and Y. Kuramoto, *Physica B* **163** (1990) 443.
- 60) E. Müller-Hartmann and A. Reischl, *Eur. Phys. J. B* **28** (2002) 173.
- 61) A. Reischl, E. Müller-Hartmann and G. S. Uhrig, *Phys. Rev. B* **70** (2004) 245124.
- 62) J. Lorenzana, J. Eroles and S. Sorella, *Phys. Rev. Lett.* **83** (1999) 5122.
- 63) R. Coldea, S. M. Hayden, G. Aeppli, T. G. Perring, C. D. Frost, T. E. Mason, S. W. Cheong and Z. Fisk, *Phys. Rev. Lett.* **86** (2001) 5377.
- 64) A. A. Katanin and A. P. Kampf, *Phys. Rev. B* **66** (2002) 100403.
- 65) M. Matsuda, K. Katsumata, R. S. Eccleston, S. Brehmer and H.-J. Mikeska, *Phys. Rev. B* **62** (2000) 8903.
- 66) M. Windt, M. Grüninger, T. Nunner, C. Knetter, K. Schmidt, G. S. Uhrig, T. Kopp, A. Freimuth, U. Ammerahl, B. Büchner and A. Revcolevschi, *Phys. Rev. Lett.* **87** (2001) 127002.
- 67) T. Nunner, P. Brune, T. Kopp, M. Windt and M. Grüninger, *Phys. Rev. B* **66** (2002) 180404.
- 68) D. Reznik, P. Bourges, H. F. Fong, L. P. Regnault, J. Bossy, C. Vettier, D. L. Milius and I. A. Aksay, *Phys. Rev. B* **53** (1996) R14741.
- 69) S. M. Hayden, G. Aeppli, T. G. Perring, H. A. Mook and F. Dogan, *Phys. Rev. B* **54** (1996) R6905.
- 70) M. Grüninger, D. van der Marel, A. Damascelli, A. Erb, T. Nunner and T. Kopp, *Phys. Rev. B* **62** (2000) 12422.
- 71) C. Knetter, K. P. Schmidt, M. Grüninger and G. S. Uhrig, *Phys. Rev. Lett.* **87** (2001) 167204.
- 72) K. P. Schmidt, H. Monien and G. S. Uhrig, *Phys. Rev. B* **67** (2003) 184413.
- 73) K. P. Schmidt and G. S. Uhrig, *Phys. Rev. Lett.* **90** (2003) 227204.
- 74) T. Barnes, E. Dagotto, J. Riera and E. S. Swanson, *Phys. Rev. B* **47** (1993) 3196.
- 75) T. Barnes and J. Riera, *Phys. Rev. B* **50** (1994) 6817.
- 76) S. Trebst, H. Monien, C. J. Hamer, Z. Weihong and R.R.P. Singh, *Phys. Rev. Lett.* **85** (2000) 4373.
- 77) P. Dai, H. A. Mook, S. M. Hayden, G. Aeppli, T. G. Perring, R. D. Hunt and F. Dogan, *Science* **285** (1999) 1344.
- 78) S. Pailhès, Y. Sidis, P. Bourges, C. Ulrich, V. Hinkov, L. P. Regnault, A. Ivanov, B. Liang, C. T. Lin, C. Bernhard and B. Keimer, *Phys. Rev. Lett.* **91** (2003) 237002.
- 79) P. Dai, H. A. Mook, R. D. Hunt and F. Dogan, *Phys. Rev. B* **63** (2001) 054525.
- 80) K. McElroy, D.H. Lee, J. E. Hoffman, K. M. Lang, J. Lee, E. W. Hudson, H. Eisaki, S. Uchida and J. C. Davis, *cond-mat/0406491*.